A granular-physics-based view of fault friction experiments

Behrooz Ferdowsi[1], **Allan M. Rubin**[1]

[1]Department of Geosciences, Princeton University, Princeton, NJ 08544, USA

Key Points:

- We examined the behavior of a sheared granular layer with time-independent contact-scale properties at and away from steady state.
- Like gouge samples in the lab, the layer mimics the rate-state friction Slip law in velocity-step and slide-hold (but not reslide) tests.
- A normalized granular temperature can be used to estimate the amplitude of the direct velocity-dependence of friction in the gouge layer.

Corresponding author: Behrooz Ferdowsi, behrooz@princeton.edu

Abstract

Rate- and State-dependent Friction (RSF) equations are commonly used to describe the time-dependent frictional response of fault gouge to perturbations in sliding velocity. Among the better-known versions are the Aging and Slip laws for the evolution of state. Although the Slip law is more successful, neither can predict all the robust features of lab data. RSF laws are also empirical, and their micromechanical origin is a matter of much debate. Here we use a granular-physics-based model to explore the extent to which RSF behavior, as observed in rock and gouge friction experiments, can be explained by the response of a granular gouge layer with time-independent properties at the contact scale. We examine slip histories for which abundant lab data are available, and find that the granular model (1) mimics the Slip law for those loading protocols where the Slip law accurately models laboratory data (velocity-step and slide-hold tests), and (2) deviates from the Slip law under conditions where the Slip law fails to match laboratory data (the reslide portions of slide-hold-slide tests), in the proper sense to better match those data. The simulations also indicate that state is sometimes decoupled from porosity in a way that is inconsistent with traditional interpretations of "state" in RSF. Finally, if the "granular temperature" of the gouge is suitably normalized by the confining pressure, it produces an estimate of the direct velocity effect (the RSF parameter a) that is consistent with our simulations, and in the ballpark of lab data.

1 Introduction

Models for estimating the length and time scales of earthquake nucleation rely on a mathematical description of the evolution of local fault friction with time (J. H. Dieterich, 1992; J. H. Dieterich & Kilgore, 1996). The commonly accepted framework for modeling this behavior, at least at sliding speeds too small for thermal effects to become important, is "Rate and State-dependent Friction", or RSF (J. H. Dieterich, 1978, 1979; J. H. Dieterich et al., 1981; A. Ruina, 1983; J. Dieterich, 1994; Marone, 1998b). The RSF framework embodies the notion that frictional strength depends upon a nebulous property termed "state", a function of recent slip history, as well as the current slip rate. Several versions of rate- and state-dependent friction laws exist, but the two most popular ones are the slip-dependent "Slip law", which does a better job matching lab data, and the time-dependent "Aging law", which matches less data (Bhattacharya et al., 2015, 2017), but which has more published theoretical justifications (e.g., Baumberger & Caroli, 2006). However, none of the existing RSF laws reproduce all of the robust features of available laboratory data (Bhattacharya et al., 2017; Kato & Tullis, 2001). This shortcoming, coupled with the largely empirical nature of RSF, severely limits our ability to apply laboratory-derived friction laws to fault slip in the Earth.

In this paper, we adopt the working hypothesis that rock friction is governed by the behavior of a granular gouge with constant Coulomb friction at grain-grain contacts. Note that by not considering time-dependent plasticity or chemical reactions at the contact scale, we are throwing out what is traditionally thought to be the source of the rate- and state-dependence of friction (e.g., J. H. Dieterich & Kilgore, 1994; Baumberger & Caroli, 2006); all the relevant time dependence in our simulations arises from momentum transfer between the gouge particles, even at very low slip speeds. We use the discrete element method to investigate the behavior of a 3-D granular layer sheared at constant normal stress between two rigid and parallel blocks. The model geometry and loading conditions are designed to mimic laboratory rock and gouge friction experiments (we note that laboratory experiments on even initially bare rock surfaces develop, through mechanical wear, either a granular powder or a granular gouge layer, depending upon the total slip distance, and that the phenomenology of RSF is common to both those experiments that start with bare rock and those where gouge is used as the starting material (Marone, 1998b)). In this paper we emphasize velocity-step tests, employing a range of shearing velocities (10^{-5} to 2 m/s) and confining pressures ($1-25$ MPa) to model steps of $\pm 1-3$ orders of magnitude. These velocity steps are supplemented by a small number of slide-hold and slide-hold-slide tests designed to allow additional comparisons to laboratory experiments and provide further insight into the gouge behavior.

Consistent with RSF and several earlier numerical studies of sheared granular layers, we find that in response to imposed velocity steps there is an immediate "direct velocity effect" (e.g., an increase in friction in response to a step velocity increase), followed by a more gradual "state evolution effect" where the sign of the friction change is reversed (Morgan, 2004; Hatano, 2009; Abe et al., 2002; Makse et al., 2004). Furthermore, the magnitudes of these direct and evolution effects are proportional to the logarithm of the velocity jump, with implied values of the relevant RSF parameters ('a' and 'b') that are not far from lab values.

Perhaps our most significant finding is that the granular flow model mimics the Slip state evolution law for those sliding protocols where the Slip law does a good job matching laboratory experiments, and deviates from the Slip law, in the proper sense to better match lab data, for those sliding protocols where the Slip law does a poor job. The former category includes both velocity-step tests (A. L. Ruina, 1980; A. Ruina, 1983; Tullis & Weeks, 1986; Marone, 1998a; Blanpied et al., 1998; Rathbun & Marone, 2013; Bhattacharya et al., 2015) and slide-hold tests (Bhattacharya et al., 2017). Consistent with both lab experiments and the Slip law, and unlike the Aging law, following a simulated velocity step friction approaches its future steady-state value over slip distances that are independent of both the magnitude and sign of the step (a few grain diameters, in our simulations, or strains of ∼15 %). And consistent with lab experiments, during the hold portion of simulated slide-hold tests stress decays in a manner consistent with the Slip law using RSF parameters not far from those derived from the velocity-step tests, whereas the Aging law, with its time-dependent healing, underestimates the stress decay. Moreover, during the simulated hold the gouge layer compacts roughly as the logarithm of hold time, similar to lab experiments. This is despite the fact that the stress decay, being well-modeled by the Sip law, implies a lack of state evolution. Because state evolution in RSF is traditionally thought to involve the "mushrooming" of contacting asperities and porosity reduction, this indicates that in both the granular simulations and the lab, state is decoupled from gouge thickness (porosity) in a way that is inconsistent with most current interpretations of RSF.

The granular flow model differs from the Slip law prediction during the reslides following holds, in that the Slip law parameters that fit the hold well underestimate the peak stress upon the reslide. Qualitatively, this is the same way in which the Slip law fails to match laboratory data (Bhattacharya et al., 2017). Collectively, our results hint that the physics-based granular flow model may do a better job of matching the transient response of laboratory rock and gouge friction experiments than any existing empirical RSF constitutive law. This is despite having apparently fewer tunable parameters. Although the model contains a large number of dimensionless parameters, most of these are fixed by the boundary conditions and the elastic moduli of the gouge particles, and the remainder seem to exert very little influence on the frictional behavior of the system. An exception is the grain size distribution; we find that a quasi-normal distribution gives rise to steady-state velocity-strengthening behavior, whereas quasi-exponential distribution close to velocity-neutral, perhaps transitioning from velocity-weakening to velocity-strengthening behavior with increasing slip speed. Grain shape may also play a significant role, but only spherical grains are employed here.

The granular model is also well-suited to allowing us to explore the microphysical origins of its RSF-like behavior. In Section 5.4 we begin to address this question, by measuring the kinetic energy of the gouge layer for a range of shear velocities, confining pressures and system sizes. By assuming that this kinetic energy plays the role of temperature in the classical understanding of the rate dependence of friction as a thermally-activated Arrhenius processes (Rice et al., 2001; Lapusta et al., 2000; Chester, 1994; Nakatani, 2001), we obtain an estimate of the magnitude of the direct velocity effect (the RSF parameter a) that is close to that determined by fitting the simulated velocity steps.

In exploring the granular model our intent is not to imply that time-dependent contact-scale processes do not contribute to laboratory friction. Clear evidence of time-dependent contact plasticity comes from the see-through experiments of J. H. Dieterich and Kilgore (1994), and evidence of the importance of chemistry and time-dependent interfacial chemical bond formation comes from, among many other studies, the humidity-controlled gouge experiments of Frye and Marone (2002), and the atomic-force single-asperity slide-hold-slide experiments of Q. Li et al. (2011). It is not yet clear, however, under what conditions such effects dominate the transient frictional strength of interfaces. Nearly all papers that justify a state evolution law on physical grounds do so for the Aging law (e.g., time-dependent plasticity increasing contact area as log time; Berthoud et al., 1999; Baumberger & Caroli, 2006), even though this law reproduces relatively little laboratory friction data. An exception is Sleep (2006), who proposed that the Slip law arises from the highly nonlinear stress-strain relation at contacting asperities. Here we explore a physics-based model that may do a better job of matching (room temperature and humidity) laboratory rock and gouge friction data than any constitutive law currently in use, and that simultaneously allows one to investigate the attributes of the model that give rise to this behavior.

2 Rate- and State-Dependent Friction background

Rate- and state-dependent friction laws treat friction as a function of the sliding rate, V, and the "state variable", θ. θ has traditionally been thought of as a proxy for true contact area on the sliding interface (Nakatani, 2001), but it has recently been shown that under some circumstances time-dependent contact quality can be the dominant contributor to the evolution of state (Q. Li et al., 2011). In its simplest form, RSF is described by two coupled, first order, ordinary differential equations. The first describes the relation between friction μ, defined as the ratio of shear stress to normal stress, and the RSF variables:

$$\mu = \mu_* + a \log \frac{V}{V_*} + b \log \frac{\theta}{\theta_*} , \tag{1}$$

where μ_* is the nominal steady-state coefficient of friction at the reference velocity V_* and state θ_*. The coefficients a and b control the magnitude of velocity- and state-dependence of the frictional strength, respectively. The second equation describes the evolution of the state variable θ, the two most widely used forms being

$$\text{Aging Law:} \quad \frac{d\theta}{dt} = 1 - \frac{V\theta}{D_c} \tag{2}$$

$$\text{Slip Law:} \quad \frac{d\theta}{dt} = -\frac{V\theta}{D_c} \ln \frac{V\theta}{D_c} \tag{3}$$

with D_c being some characteristic slip distance (J. H. Dieterich, 1979; A. Ruina, 1983). Eq. 2 is often referred to as the Aging law since state can evolve with time in the absence of slip; Eq. 3 is referred to as the Slip law since state evolves only with slip ($\dot{\theta} = 0$ when $V = 0$).

It is well established that neither the Aging law nor the Slip law adequately describes the full range of laboratory friction experiments (Beeler et al., 1994; Kato & Tullis, 2001). Laboratory experiments show that in a sufficiently stiff system, for both initially bare rock samples and gouge, following a step change in load point velocity friction approaches its new steady-state value quasi-exponentially over a characteristic slip distance that is independent of both the magnitude and the sign of the velocity step (A. Ruina, 1983; Marone, 1998b; Blanpied et al., 1998; Bhattacharya et al., 2015). This is precisely the Slip law prediction of state evolution (Nakatani, 2001). The Aging law, on the other hand, predicts a slip weakening distance that increases as the logarithm of the velocity jump for step velocity increases, and, owing to the approximately linear increase of state with time, exceedingly small slip distances for frictional strength recovery following large step velocity decreases. Both behaviors are completely inconsistent with laboratory data (Nakatani, 2001).

In contrast, conventional wisdom holds that slide-hold-slide experiments are better explained by the Aging law. In part this stems from the work of Beeler et al. (1994), who ran experiments on initially bare granite surfaces at two different machine stiffnesses, and hence two different amounts of slip during the load-point holds. They found that the rate of healing, as inferred from the peak stress upon the reslide, was independent of stiffness, and hence independent of the small amount of interfacial slip during the load-point holds, seemingly consistent with the Aging law and inconsistent with the Slip law. However, Bhattacharya et al. (2017) showed that the Beeler et al. peak stress data could be fit about as well by the Slip law as by the Aging law, and moreover that the stiffness-dependent stress decay during the load-point holds could be well modeled by the Slip law, although with a slightly different value of $(a-b)$ than was determined from contemporaneous velocity steps, and was completely inconsistent with the Aging law. The property of the Aging law that prevents it from matching the stress decay during the holds is precisely its time-dependent nature: The gouge strengthens too much to allow any more slip. The rock friction community is thus left in the awkward position that while most theoretical justifications for state evolution are designed to explain the time-dependent healing of the Aging law (e.g., Baumberger et al., 1999), this law seems to explain rather little laboratory rock friction data.

3 The computational model

Our Discrete Element Method (DEM) simulations are performed using the *granular* module of LAMMPS (Large scale Atomic/Molecular Massively Parallel Simulator), a multi-scale computational platform developed and maintained by Sandia National Laboratory (`http://lammps.sandia.gov`). What we will refer to as the "default" model consists of a packing of 4815 grains: 4527 in the gouge layer, and 288 in the top and bottom rigid blocks. The grains in the gouge layer have a polydisperse normal-like size distribution (Figure 1B), with a diameter range $d = [1:5]$ mm and average diameter $D_{mean} = 3$ mm (Figure 1A). The granular gouge is confined between two parallel and rigid plates that are constructed from grains with diameter $d = 5$ mm. Grain density and Young's modulus are chosen equal to properties of glass beads (Table 1). The model domain is rectangular with periodic boundary conditions applied in the x and y directions. The size of the system in each direction is $L_x = L_y = 1.5L_z = 20\ D_{mean}$.

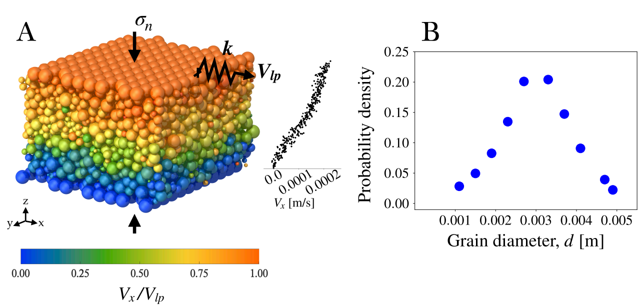

Figure 1. (A) A visualization of the "default" granular gouge simulation. A normal grain size distribution is used, with mean grain diameter $D_{mean} = 3$ mm. Colors show the velocity of each grain in the x direction, averaged over an upper-plate sliding distance of D_{mean} during steady sliding at a driving velocity of $V_{lp} = 2\times10^{-4}$ m/s. The actual velocity profile, averaged over 400 planes normal to z, is shown to the right (black dots). (B) The size distribution of grains in the gouge layer in the default model.

The system is initially prepared by randomly inserting (under gravity) grains in the simulation box with a desired initial packing fraction of ∼0.5. The system is then allowed to relax for about 10^6 time steps, after which three initially identical and relaxed realizations are subjected to confining pressures $\sigma_n = [1,5,25]$ MPa. The confining pressure is applied for one minute, by which time the fast phase of compaction is completed. These confined gouge samples are then subject to shearing at a desired driving velocity imposed by the top rigid plate, while the vertical position of the top wall is adjusted by a servo-control system to maintain the specified (constant) confining pressure. We find that the servo-control system keeps the normal stress constant to within about ±0.1% of the desired value at slip speeds of 0.1 m/s (see supplementary Figure S2 for an example of the servo control during and following a velocity step), and that the variation about the desired value is reduced by about a factor of 5 at slip speeds 5 times smaller. The non-default systems are prepared using an identical protocol at a confining pressure of $\sigma_n = 5$ MPa. The driving velocity is applied to the system via a linear spring with a default stiffness of 10^{14} N/m attached to the top plate; for practical purposes, this stiffness can be considered to be infinite, in that changes in load point velocity are transferred nearly instantaneously to the upper plate. The grains are modeled as compressible spheres of diameter d that interact when in contact via the Hertz-Mindlin model (K. L. Johnson, 1987; Landau & Lifshitz, 1959; Mindlin, 1949).

For two contacting particles $\{i, j\}$, at positions $\{\boldsymbol{r}_i, \boldsymbol{r}_j\}$, with diameters d_i and d_j, velocities $\{\boldsymbol{v}_i, \boldsymbol{v}_j\}$ and angular velocities $\{\omega_i, \omega_j\}$, the force on particle i is computed as follows: The normal compression δ_{ij}, relative normal velocity $\boldsymbol{v}_{n_{ij}}$, and relative tangential velocity $\boldsymbol{v}_{t_{ij}}$ are given by

$$\delta_{ij} = \tfrac{1}{2}(d_i + d_j) - r_{ij} \tag{4}$$

$$\boldsymbol{v}_{n_{ij}} = (\boldsymbol{v}_{ij} \cdot \boldsymbol{n}_{ij})\boldsymbol{n}_{ij} \tag{5}$$

$$\boldsymbol{v}_{t_{ij}} = \boldsymbol{v}_{ij} - \boldsymbol{v}_{n_{ij}} - \tfrac{1}{2}(\boldsymbol{\omega}_i + \boldsymbol{\omega}_j) \times \boldsymbol{r}_{ij} \tag{6}$$

where $\boldsymbol{r}_{ij} = \boldsymbol{r}_i - \boldsymbol{r}_j$, $\boldsymbol{n}_{ij} = \boldsymbol{r}_{ij}/r_{ij}$, with $r_{ij} = |\boldsymbol{r}_{ij}|$, and $\boldsymbol{v}_{ij} = \boldsymbol{v}_i - \boldsymbol{v}_j$. The rate of change of the elastic tangential displacement $\boldsymbol{u}_{t_{ij}}$, set to zero at the initiation of a contact, is given by

$$\frac{d\boldsymbol{u}_{t_{ij}}}{dt} = v_{t_{ij}} - \frac{(\boldsymbol{u}_{t_{ij}} \cdot \boldsymbol{v}_{ij})}{r_{ij}^2} \tag{7}$$

where the second term in equation 7 comes from the rigid body rotation around the contact point. Its implementation is there to insure that $\boldsymbol{u}_{t_{ij}}$ always locates in the local tangent plane of contact (Silbert et al., 2001). The normal and tangential forces acting on particle i are then given by:

$$\boldsymbol{F}_{n_{ij}} = \sqrt{\delta}_{ij}\sqrt{\frac{d_i d_j}{2(d_i + d_j)}}(k_n \delta_{ij} \boldsymbol{n}_{ij} - m_{eff}\gamma_n \boldsymbol{v}_{n_{ij}}) \tag{8}$$

$$\boldsymbol{F}_{t_{ij}} = \sqrt{\delta}_{ij}\sqrt{\frac{d_i d_j}{2(d_i + d_j)}}(-k_t \boldsymbol{u}_{t_{ij}} - m_{eff}\gamma_t \boldsymbol{v}_{t_{ij}}) \tag{9}$$

where k_n and k_t are the normal and tangential stiffness, given by $k_n = (2/3)E/(1 - \nu^2)$ and $k_t = 2E/(1+\nu)(2-\nu)$ (Mindlin, 1949), with E being Young's modulus and ν Poisson's ratio, and $m_{eff} = m_i m_j/(m_i + m_j)$ is the effective mass of spheres with masses m_i and m_j (we note that the most appropriate value of k_t seems to be a matter of some debate, with Shäfer et al. (1996) suggesting values roughly 1000 times smaller). γ_n and γ_t are the normal and tangential damping (viscoelastic) constants, respectively; we maintain the default LAMMPS option of $\gamma_t = 0.5\gamma_n$. As indicated by equations 8 and 9, the model implements damping for both normal and tangential contacts as a spring and dashpot in parallel. Note that the Hertzian normal force given by (8) increases non-linearly with grain compression δ_{ij} (equation 4), as $\delta_{ij}^{3/2}$ in the absence of damping, consistent with the elastic deformation of contacting spheres.

In a gravitational field $\boldsymbol{g}$, the translational and rotational accelerations of particles are determined by Newton's second law, in terms of the total forces and torques on each particle, i:

$$\boldsymbol{F}_i^{tot} = m_i \boldsymbol{g} + \sum_j \left(\boldsymbol{F}_{n_{ij}} + \boldsymbol{F}_{t_{ij}}\right) \tag{10}$$

$$\boldsymbol{\tau}_i^{tot} = -\frac{1}{2}\sum_j \boldsymbol{F}_{t_{ij}} \times \boldsymbol{r}_{ij} \tag{11}$$

The grain-grain coefficient of friction, μ_g, is the upper limit of the tangential force through the Coulomb criterion $F_t \leq \mu_g F_n$. The tangential force between two grains grows according to the non-linear Hertz-Mindlin contact law until $F_t/F_n = \mu_g$ and is then held at $F_t = \mu_g F_n$ until either $F_t \leq \mu_g F_n$ or the grains loose contact.

The amount of energy lost in collisions is characterized by the coefficient of restitution. The values of restitution coefficients, ϵ_n and ϵ_t for the normal and tangential directions respectively, are related to their respective damping coefficients $\gamma_{n,t}$ and contact stiffness $k_{n,t}$. The restitution coefficient for the normal direction can be calculated by solving the following equation that describes the normal component of the relative motion of two spheres in contact:

$$\ddot{\delta} + \frac{E\sqrt{2d_{eff}}}{3m_{eff}(1-\nu^2)}\left(\delta^{3/2} + \frac{3}{2}A\sqrt{\delta}\dot{\delta}\right) = 0 \tag{12}$$

with the initial conditions $\dot{\delta}(0) = \boldsymbol{v}_n$ and $\delta(0) = 0$. In this equation, $A = \frac{1}{3}\frac{(3\gamma_t-\gamma_n)^2}{(3\gamma_t+2\gamma_n)}\left(\frac{(1-\nu^2)(1-2\nu)}{E\nu^2}\right)$, and $d_{eff} = d_i d_j/(d_i + d_j)$ is the effective diameter for spheres of diameters d_i and d_j. The normal component of the coefficient of restitution can be obtained from the ratio of normal velocity of grains at the end of the collision, defined as $\dot{\delta}(t_{col})$, to their initial normal impact velocity: $\epsilon_n = \dot{\delta}(t_{col})/\dot{\delta}(0)$. The collision time t_{col} is determined by solving Eq. 12 for the adopted physical properties and initial velocities of two colliding grains. A similar procedure is performed for calculating the restitution coefficient in the tangential direction. We use a time step of $\Delta t = t_{col}/100$ throughout this study, with t_{col} evaluated assuming an impact velocity $\dot{\delta}(0)$ of 25 m/s (t_{col} in (12) depends very weakly upon $\dot{\delta}(0)$, as roughly $\dot{\delta}(0)^{1/5}$ (Shäfer et al., 1996)). The restitution coefficient in the default model is chosen to be very high ($\epsilon_n = 0.98$), such that the system is damped minimally. Although in one sense damping introduces time-dependence at the contact scale, we find by varying the restitution coefficients from nearly zero (complete damping) to nearly 1 (no damping) that they exert no significant influence on the system behavior in the slow-sliding regime of interest. For this reason we refer to the model as having no time-dependence at the contact scale. The full details of the granular module of LAMMPS are described in the LAMMPS manual and several references (Zhang & Makse, 2005; Silbert et al., 2001; Brilliantov et al., 1996).

In addition to the default model, we have run simulations with a domain size twice the size of the default model, simulations with a grain and domain size two orders of magnitude smaller, simulations with grain-grain friction coefficients of 1.0 and 5.0 (default = 0.5), simulations with restitution coefficients ϵ_n of 0.003 to 0.82 (default = 0.98), and simulations with either a quasi-exponential grain size distribution. The influence of most of these changes on the model results are rather modest, and we relegate detailed figures to the supplementary materials of this manuscript. An exception are the models with a different grain size distribution; these are described in section 5.2.6. A full accounting of the dimensionless parameters governing the model is provided in Appendix A. In principle, we wanted to prepare models that could isolate the influence of each parameter that we tested. However, because of the way we used the LAMMPS random particle generator, in some cases there are slight variations in the total number of particles, which are reflected in different values of L_z (hereafter referred to as the gouge thickness H). Compared to the default model, for the simulations with different grain-grain friction coefficients H is larger by 10%; for the simulations with a grain and domain size two orders of magnitude smaller the ratio H/D_{mean} is larger by 7%, and in the simulations where L_x and L_y are two times larger, H is only 1.8 times larger (we continue to refer to this as the "two-times larger" model).

Table 1. DEM simulation parameters. The "default model" values, where multiple values are given, are in bold font.

Parameter	Value
Grain density, ρ	2500 [kg/m^3]
Young's modulus, E	50 [GPa]
Poisson ratio, ν	0.3
Grain-grain friction coefficient, μ_g	**0.5**, 1.0, 5.0
Confining pressure, σ_n	1, **5**, 25 [MPa]
Coefficient of restitution, ϵ_n	**0.98**, 0.82, 0.25, 0.01, 0.003
Time step, Δt	2×10^{-8} [s]

The velocity V in the RSF equations (1)–(3) is interpreted in laboratory experiments as the inelastic component of the relative tangential displacement rate between two parallel planes. This displacement rate is typically treated conceptually as occurring across a plane of zero thickness, but in fact it occurs across a zone whose thickness is generally unknown. In lab experiments, the relative displacement is measured between two points outside the zone of inelastic deformation, and the inelastic component of that displacement δ is determined by subtracting the estimated elastic displacement δ_{el} from the measured (total) displacement, i.e.

$$\begin{aligned} \delta &= \delta_{lp} - \delta_{el} = \delta_{lp} - \tau/k \,, \\ \tau &= k(\delta_{lp} - \delta) \,, \end{aligned} \tag{13}$$

where δ_{lp} is the measured "load-point" displacement (in our simulations the displacement of the end of the spring not attached to the upper plate), τ the spring force divided by the nominal sample surface area (6 cm $\times$ 6 cm in our default model), and k the elastic stiffness of the combined testing apparatus plus sample between the measurement points. In our numerical simulations this stiffness is given by the effective stiffness of two springs in series,

$$k_{\text{eff}} = \frac{k_{sp} k_H}{k_{sp} + k_H} \,, \tag{14}$$

where k_{sp} and k_H are the spring and gouge stiffness, respectively. To measure k_H, we performed several slide-hold-reslide simulations with a range of hold durations (Figure B1). The shear modulus can be estimated from the initially linear (assumed to be elastic) portion of the reslide following the longest holds in such simulations (e.g., Bhattacharya et al., 2017). From these tests, the shear modulus of the gouge layer is estimated to be in the range of $G_H \approx 270$ to 310 MPa, at a confining pressure of 5 MPa. This estimate is about 30 – 50% lower than previous experimental measurements on granular layers made from packing glass beads (Yin, 1993; Domenico, 1977; Makse et al., 1999), and granular simulations with properties similar to our model. However, those previous experiments and simulations were performed under specially designed preparation protocols, to produce a maximal packing fraction under a given confinement. We expect our simulation samples (that are generated under conditions similar to synthetic gouge experiments) to have a lower packing fraction and to exhibit a lower shear modulus. Although the appropriate value of G_H may vary modestly with the sliding history and packing properties of the gouge, we neglect this possibility here. For G_H from 270 to 310 MPa, the stiffness k_H varies from $G_H/H = 6.75 \times 10^9$ to 7.75×10^9 Pa/m, where $H = 0.04$ m is the gouge thickness. To determine k_{sp} in Pa/m from the stiffness input in LAMMPS in units of N/m, we divide by the sample surface area. For the default spring stiffness of 10^{14} N/m, $k_{sp} \sim 3 \times 10^{16}$ Pa/m $\gg k_H$, so $k_{\text{eff}} \sim k_H$. This value of k_{eff} is so large that even large errors in G_H play no role in the Slip law fits to our simulated velocity steps (k_{eff} is essentially infinite).

Using (13) and (14) ensures that our analysis is consistent with both the conventional interpretation of equations (1)–(3) and standard laboratory protocols. For example, with k_{sp} essentially infinite and V_{lp} set to zero (a "hold"), the upper plate remains stationary, but due to granular rearrangements within the gouge the inelastic displacement δ increases and $V > 0$ as the stress relaxes.

4 Previous studies of granular rheology related to rock friction

The granular model has many dimensionless parameters, but most turn out to be unimportant in the region of parameter space of interest (Appendix A). Within the physics literature, the most important is understood to be the Inertial number, defined as

$$I_n \equiv \dot{\gamma} D_{mean} \sqrt{\rho/P} \approx \frac{V}{H} D_{mean} \sqrt{\rho/P}, \tag{15}$$

where $\dot{\gamma}$ is the local shear rate (approximated as the slip speed divided by the gouge thickness in the second expression), P is the confining pressure (or normal stress, for the geometry of our simulations), and ρ and D_{mean} are the density and mean diameter of grains, respectively. The inertial number measures the ratio of the inertial forces of grains to the confining forces acting on those grains, such that small values ($I_n \lessapprox 10^{-3}$) correspond to the quasi-static state. A continuum model that has proven moderately successful in modeling steady-state granular friction is known as $\mu(I_n)$ rheology (Forterre & Pouliquen, 2008), where the local coefficient of friction depends only upon the local inertial number. However, in some regions of parameter space the dimensionless pressure, defined as $\bar{P}_{\text{Hertz}} \equiv (P/E)^{2/3}$ for the Hertzian contact law that we use, and as $\bar{P}_{\text{Hook}} \equiv PD_{mean}/k_{\text{grain}}$ for a linear ($F_n \propto \delta_{ij}$) Hookean contact law (appropriate for 2-D simulations, with k_{grain} being the adopted grain-grain spring stiffness), also plays a role. Both versions of $\bar{P}$ are proportional to the nominal elastic strain of grains subjected the applied load, given the adopted contact law (Salerno et al., 2018; DeGiuli & Wyart, 2017), and we only distinguish between them when necessary. For granular gouge with a quartz-like modulus ($E \sim 50$ to 70 GPa) and normal stresses from 2 to 50 MPa, $\bar{P}_{\text{Hertz}}$ varies from $\sim 10^{-3}$ to 10^{-2}; the "rigid grain" (undeforming) limit is thought to be reached in the limit $\bar{P} \lesssim 10^{-3}$ (DeGiuli & Wyart, 2017; de Coulomb et al., 2017).

The steady-state behavior of sheared granular layers has been studied extensively in the past two decades, using both simulations and experiments. Most numerical studies have explored values of I_n from roughly 10^{-5} to 10^0, crossing the quasi-static to inertial transition. These studies generally find steady-state friction to be well fit by a power-law of the form $\mu_{ss} = \mu_0 + b I_n{}^{\alpha}$, with μ_0, b and α being fitting parameters. When plotted vs $\log(I_n)$ or $\log(V)$, friction is strongly velocity(rate)-strengthening within the inertial regime, transitioning to weakly velocity-strengthening and ultimately asymptoting to velocity-neutral with decreasing I_n within the quasi-static regime (da Cruz et al., 2005; de Coulomb et al., 2017; Kamrin & Koval, 2014; Hatano, 2007). In contrast, some laboratory studies of sheared granular flow find velocity-weakening behavior within the quasi-static regime (Dijksman et al., 2011; Kuwano et al., 2013; G. H. Wortel et al., 2014), but potentially this could be due to time-dependent contact-scale processes not accounted for in the numerical simulations. However, in a theoretical study DeGiuli and Wyart (2017) concluded that a sheared 2-D granular layer with a Hookean contact law changes behavior from velocity-strengthening for $I_n \gtrsim 10^{-3}$ to slightly velocity-weakening at lower I_n, asymptoting to velocity-neutral as I_n decreases further, provided $\bar{P} \lesssim 10^{-3}$.

Studies of granular gouge layers away from steady state are much less common and are mostly restricted to the geological literature. Using a model of a sheared granular fault gouge, Morgan (2004) observed both the direct and state evolution effects in velocity-stepping tests, and the logarithmic-with-time healing of friction upon resliding in slide-hold-slide tests. In those simulations Morgan introduced a time-dependent grain-grain contact law, with $\mu_g \propto \log[\text{contact time}]$. Likewise, Abe et al. (2002) implemented the Slip law version of state evolution to describe the time-dependence of the grain-grain friction coefficient in slide-hold-slide simulations, and again observed logarithmic healing of friction with time upon resliding. Because both of these studies introduced time-dependence at the contact scale, it is difficult to isolate the purely geometrical contribution of granular flow to the transient frictional behavior they observed. Furthermore, neither study compared their results to laboratory experiments at the level of detail required, for example, to distinguish between competing state evolution laws. Hatano (2009) simulated velocity-stepping experiments, in 3 dimensions but using a linear (Hookean) contact law for grain-grain interactions, for a range of inertial numbers $10^{-5} \lessapprox I_n \lessapprox 10$, and dimensionless pressures $10^{-5} \lesssim \bar{P} \lesssim 10^{-1}$. He observed a critical slip distance that scaled linearly with the size of the velocity steps, behavior that is not reproduced by our simulations and that is also inconsistent with laboratory rock friction experiments.

In the RSF framework, a steady-state velocity-weakening system and a system stiffness below a critical value are necessary conditions for stick-slip motion. Using a very soft spring for applying the sliding velocity ($k_{\text{spring}} \sim 3 \times 10^{-5} k_{\text{grain}}$, where k_{grain} is grain stiffness), Aharonov and Sparks (2004) performed DEM simulations of a two dimensional confined sheared granular layer for $6 \times 10^{-4} \lesssim I_n \lesssim 0.2$ and $10^{-5} \lesssim \bar{P} \lesssim 10^{-3}$. They showed that the frictional behavior changes from stick-slip to oscillatory motion to steady-sliding as I_n increases. Similar behavior was later reproduced by Ferdowsi et al. (2013). Neither Aharonov and Sparks (2004) nor Ferdowsi et al. (2013) directly measured the steady-state friction coefficient as a function of velocity, so it is not clear if their systems were in the rate-weakening regime when stick-slip behavior emerged, or whether in granular systems stick-slip may occur despite the system being rate-strengthening. One could imagine, for example, that with a sufficiently soft spring and a system small enough for only a small number of force chains to develop, collapse of a force chain might lead to sudden accelerations. The existence, origins and controls of a transition from rate-weakening to rate-strengthening behavior in sheared granular layers is still a matter of much debate (Perrin et al., 2019; van Hecke, 2015). Recent experimental and numerical studies show that the variation of friction coefficient with shear rate and inertial number depends on the grain shape, surface roughness, and size distribution (Mair et al., 2002; Salerno et al., 2018; Murphy, Dahmen, & Jaeger, 2019; Murphy, MacKeith, et al., 2019). In our preliminary results examining the influence of grain size distribution, we find that the behavior changes from velocity strengthening to approximately velocity neutral when the grain size distribution is changed from quasi-normal to quasi-exponential.

A continuum model for the flow of amorphous materials, recently applied to granular gouge, is known as Shear Transformation Zone (STZ) theory (Lemaître, 2002; Manning et al., 2007). In response to imposed velocity steps, STZ models exhibit both a direct velocity effect and an opposing state evolution effect, consistent with lab experiments and RSF (Daub & Carlson, 2008; Lieou et al., 2017). However, STZ models have yet to be compared to lab data at the level of, for example, establishing the basic result that the slip distance for stress (or state) evolution following an imposed velocity step is independent of the magnitude and sign of that step (Bhattacharya et al., 2015). Such tests matter because, as stated previously, simply documenting that a model has a direct and an evolution effect is insufficient justification for applying it to processes such as earthquake nucleation (Ampuero & Rubin, 2008). Furthermore, in the most recent versions of STZ (Lieou et al., 2017; Ma & Elbanna, 2018), variations in the state variable ("compactivity") are assumed to be proportional to the gouge volume (thickness) change. However, both our granular simulations and laboratory friction experiments (to be discussed in section 5.2), and recent granular physics studies (Bililign et al., 2019; Puckett & Daniels, 2013) indicate that gouge thickness change is an inadequate description of state. Continuum approaches such as STZ theory may benefit from detailed studies of the granular physics of RSF of the sort described in this manuscript.

5 Results

5.1 Steady-state friction

The results of granular simulations run to quasi-steady-state at different normal stresses and driving velocities are shown in Figure 2. Because individual runs tend to be somewhat noisy, presumably due to the relatively small system size, each data point is averaged over seven different realizations (initial packings) of the granular fault gouge, and each of these realizations is averaged over a sliding distance of five times the mean grain diameter D_{mean}. Friction in this and all figures in this paper is defined as the ratio of shear to normal stress τ/σ, with τ and σ defined as the shear and normal force per unit area exerted by the gouge particles on the upper (driving) plate. This definition ensures that we are measuring the frictional strength of the gouge at the boundary with the upper plate, should that differ from the applied spring force (any mismatch leading to acceleration of the

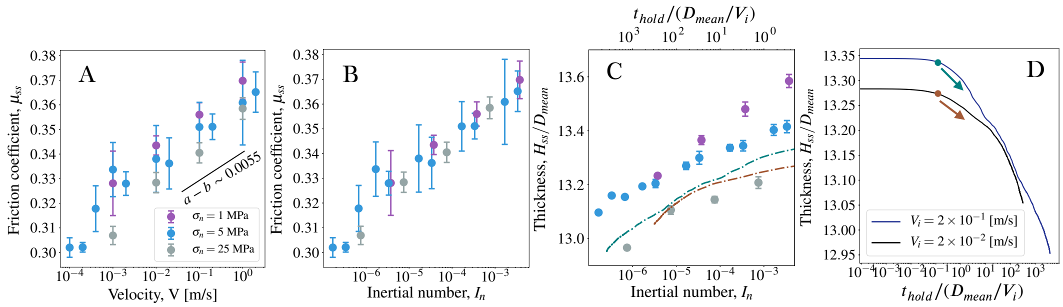

Figure 2. (A) The variation of steady-state friction coefficient with driving velocity at three different normal stresses. (B) The same data plotted as a function of inertial number (I_n). (C) The variation of steady-state gouge thickness at different driving velocities as a function of I_n, for the same three normal stresses. Error bars indicate one standard deviation of all friction measurements over a sliding distance of $5D_{mean}$ for each of the seven different realizations (initial grain arrangements) at each normal stress and V_{lp}. Most error bars in (C) are smaller than the symbol size. The dashed teal and brown lines in (C) show the temporal evolution (upper horizontal axis) of gouge thickness in the hold experiments shown in panel (D). (D) The evolution of gouge thickness with time during slide-hold experiments at $V_i = 2\times10^{-1}$ and 2×10^{-2} m/s. Zero time in these plots marks the start of the hold (the halting of the upper driving plate). The teal and brown dots and arrows show the starting point and temporal progression of the curves that we plot in panel (C) (time progresses to the left in C). The confining pressure is $\sigma_n = 5$ MPa.

upper plate). In the absence of significant accelerations that are coherent when averaged over $x-y$ planes, from force balance the shear stress as we have defined it is uniform throughout the gouge.

The nominal friction coefficient in Figure 2A, ~ 0.33, is low by laboratory standards. This low value is likely due to the use of spherical grains, as laboratory studies also show mean nominal friction coefficients in the range $0.25-0.45$ for glass beads and for synthetic gouge layers produced from spherical grains (Anthony & Marone, 2005). Mair et al. (2002) also found that by changing grain shapes from smooth spherical to angular the mean steady-state friction increases from ~ 0.45 to ~ 0.6. A recent computational study by Salerno et al. (2018) further shows that using non-spherical grains shifts the dynamic friction versus inertial number curves upward uniformly, increasing mean friction values from $0.25-0.35$ for spheres to the $0.5-0.6$ range for rounded-edge cubic grains. Note that for comparison to RSF we are primarily concerned with the variations of friction with slip rate and slip history. In the absence of thermal weakening mechanisms, numerical simulations of fault slip in an elastic solid depend only upon the time-variation of friction and not its absolute value.

For our default model we find steady-state friction to vary essentially linearly with the logarithm of slip speed over the full range of parameters we have explored. Such behavior has been previously observed in solid-on-solid friction in many different materials (Baumberger et al., 1999; Berthoud et al., 1999; J. H. Dieterich, 1979; A. Ruina, 1983; Karner & Marone, 1998), as well as in experiments with spherical and non-spherical granular particles at low inertial numbers (Hartley & Behringer, 2003; Behringer et al., 2008) [although it is arguable that in experiments, time-dependent contact-scale processes may contribute to the observed logarithmic rate-dependence (Heslot et al., 1994; Nakatani, 2001)]. We find velocity-strengthening behavior over the range of parameters explored thus far, consistent with many experiments on gouge, although many other gouge experiments show nearly velocity-neutral behavior (Marone, 1998b; Marone et al., 1990). The value of $|a-b|$ from the slope of our data, ~ 0.0055, is slightly high by lab standards, but Marone et al. (1990) found values as high as 0.005 for laboratory gouge, and we emphasize that unlike standard RSF and STZ theory this value is an output of the model and not a tunable parameter.

Note that in Figure 2A the friction coefficient increases slightly with decreasing normal stress. This is not a feature of standard RSF, but it is consistent with some laboratory data (e.g., J. H. Dieterich, 1972). If the data are plotted against the inertial number I_n rather than velocity (Figure 2B), there is a near collapse of all observations onto a single curve, as expected from previous work. Relative to previous numerical studies we explore a somewhat lower range of I_n (roughly $10^{-7} - 10^{-2}$, compared to $10^{-5} - 10^{0}$). While those previous studies found steady-state friction to have a power-law dependence upon I_n, they are nonetheless consistent with ours in that for the overlapping range of I_n ($\sim 10^{-5} - 10^{-2}$) they can be fit quite well by a logarithmic dependence of friction upon I_n, with a slope not much different than ours (Hatano, 2007). It is within the inertial regime of flow, for $I_n \gtrsim 10^{-2}$, that the steady-state friction vs. $\log(I_n)$ curves in previous studies become strongly concave-up and require a power-law fit. Our steady-state results differ from previous simulations mostly in extending the range of I_n lower by ∼2 orders of magnitude, the lowest we can achieve in a few weeks of computation time. We find the logarithmic dependence to continue to those lower values, while the power-law fits adopted by previous studies continue to flatten with decreasing I_n (for further discussion see supplementary information Section 1 and supplementary Figure S1).

To estimate how our range of I_n compares to that accessed by typical laboratory gouge friction experiments, we note with reference to equation (15) that such experiments typically don't vary very far from our value of $(\rho/P)^{1/2}$. This means that if our adopted value of $D_{mean}/H \sim 1/13$ is appropriate, our simulations will have basically the same I_n as a lab experiment with the same V. The synthetic gouge experiments of Mair and Marone (1999), for example, spanned slip speeds of 0.3–3000 μm/s, compared to our lowest V of 200 μm/s. Thus, typical low-velocity lab friction experiments can be expected to overlap the lowest values of I_n we explore, but to extend to values of I_n several orders of magnitude lower still. At slip speeds within the upper half of our range, say 0.1 m/s, thermal weakening mechanisms are expected to dominate over classical RSF in rock friction experiments (e.g., Rice, 2006). To estimate I_n for the Mair and Marone (1999) experiments more precisely we can use their $P = 25$ MPa and initial value of $D_{mean}/H \approx 1/30$ (initial grain size 50–150 μm; gouge thickness 3 mm), to obtain $10^{-10} < I_n < 10^{-6}$. For experiments accompanied by grain comminution and strain localization over a thickness H_{eff}, I_n will vary to the extent that D_{mean}/H_{eff} varies from ∼1/30 (although the behavior at a given I_n could change for non-spherical particles, and if the grain size distribution becomes very large then the appropriate choice of D_{mean} in the definition of I_n might need to be re-examined). Based upon experimental studies summarized by Rice (2006), shear bands in granular sands with a relatively narrow size distribution often satisfy $D_{mean}/H_{eff} \sim 1/10 - 1/20$.

The steady-state gouge thickness H in our simulations decreases with increasing normal stress, but increases quasi-linearly with $\log(I_n)$ at a rate that is only weakly dependent on normal stress (Figure 2C). The logarithmic rate-dependence of gouge thickness, with the gouge thickness change ΔH being $\sim 0.1 D_{mean}$ per order of magnitude increase in driving velocity, also seems roughly consistent with laboratory observations (Rathbun & Marone, 2013; Beeler & Tullis, 1997; Marone & Kilgore, 1993). (We show in the next section that in our simulations $0.1 D_{mean} \sim 0.05 D_c$, which enables a comparison with lab experiments where D_c is estimated but not D_{mean}.)

The temporal evolution of the gouge layer thickness in two slide-hold simulations is shown in semi-log scale in Figure 2D. Both the friction coefficient (shown later in Figure 12A) and the gouge thickness show a relaxation with the logarithm of time. We compare the compaction rate of the gouge during the holds to the dilation rate as a function of inertial number in Figure 2C. The similar slopes of the thickness data from the steady-sliding experiments (dots) and the holds (teal and brown lines) show that the reduction in gouge thickness that results from a ten-fold increase in hold duration is comparable to the reduction from a ten-fold decrease in inertial number (∼slip speed). This suggests that the origin of the velocity-dependence of steady-state gouge thickness may lie in the same slow relaxation process that operates during holds. J. H. Dieterich (1978) proposed a somewhat analogous equivalency between increased hold duration and decreased slip speed in laboratory experiments: That contact strength increased logarithmically with age, whether that age was defined as the duration of a hold, or as the typical contact lifetime (contact dimension divided by the steady sliding speed).

5.2 Velocity step simulations

The results of several granular velocity-step simulations, with load-point velocity increases of $1-4$ orders of magnitude, are shown in Figure 3A. “Slip” on the horizontal axis in this and all subsequent figures is the inelastic displacement as defined by equations (13) and (14). The solid curves show the measured friction relative to the future steady-state value. Immediately following the velocity increase there is a stress increase, roughly proportional to the logarithm of the velocity jump, representing a direct velocity effect, followed by a quasi-exponential decay to the new steady state value, representing a state evolution effect (the system is stiff enough that V over the stress decay is essentially identical to the load-point velocity, so from equation (1) there is a linear relation between the change in friction and the change in log state following the friction peak). This friction decay occurs over a sliding distance of a few mean grain diameters.

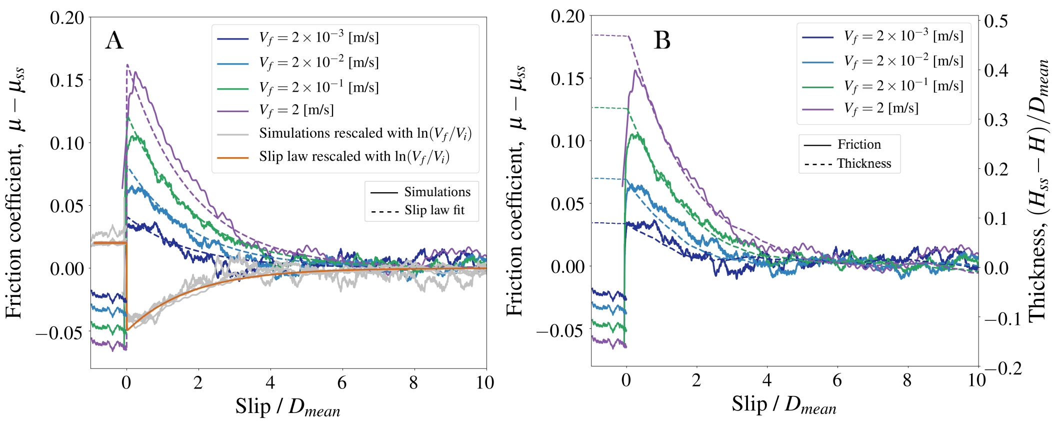

Figure 3. (A) Results from step velocity increases with initial load-point velocity $V_i = 2 \times 10^{-4}$ m/s. The friction coefficient, plotted relative to its future steady state value to emphasize the state evolution, is shown as a function of shear slip distance normalized by D_{mean}. Slip in this and later figures is defined to be zero at the time of the step. The curve for the 4-order increase to $V_f = 2$ m/s jumps discontinuously backward to a small negative slip value because equation (13) does not account for elastodynamic effects (see Appendix B). The gray curves are the friction signals rescaled as $-0.05(\mu - \mu_{ss})/b\ln(V_f/V_i)$ (the -0.05 is used just to make all signals visible on the same axis). The dashed lines show the prediction of the Slip law with $b = 0.0178$, $a = 0.0247$ and $D_c = 1.78D_{mean}$ (see text). (B) The solid lines show the variation of friction with normalized slip from panel (A). The dashed lines show the difference between the steady-state gouge thickness H_{ss} and the current thickness H, normalized by the mean grain diameter D_{mean} (the gouge dilates with slip). The results are averaged over seven different realizations of the same imposed loading conditions, with σ_n fixed at 5 MPa.

Given the increase in steady-state gouge thickness with slip speed/inertial number (Figure 2C), it seems reasonable to suggest that the direct velocity effect comes from sliding at the new (higher) slip speed but with the old (compacted) gouge thickness, while the state evolution effect is associated with the gradual approach to the new steady-state gouge thickness. A direct correspondence between state and gouge porosity has also been proposed in the context of both RSF (Segall & Rice, 1995; Sleep, 2006) and STZ theory (Lieou et al., 2017). However, although this view has some intuitive appeal, we show below that it is too simplistic; there is not a one-to-one relation between “state” and gouge thickness. (We also note here, in anticipation of results to be presented in section 5.2.2, that in simulations that use the same particle size distribution but a gouge thickness H 1.8 times larger, the gouge evolves to steady state over a slip distance roughly 1.8 times larger; that is, state evolution seems to be governed by a critical strain rather than by a critical slip distance. For convenience, we speak here of a critical slip distance. This does not alter our previous estimate of $\Delta H/D_c$ for a given log velocity change, where ΔH is the change in gouge thickness, because in our simulations both ΔH and D_c are proportional to H.)

The gray curves in Figure 3A show these friction changes normalized by the logarithm of the velocity jump, and are flipped for ease of visualization. That the gray curves all nearly overlap, that is, have approximately the same scaled amplitude and approach the new steady state over the same sliding distance, is entirely consistent with the Slip law description of state evolution with quasi-constant values of a, b, and D_c (Bhattacharya et al., 2015). Using a simplex method we find the single set of (Slip law) RSF parameters that best matches these velocity jumps to be $a \sim 0.025$, $b \sim 0.018$, and $D_c \sim 1.8D_{mean}$. These values of a and b are on the high side but are within a factor of 2 of those commonly cited for rock and gouge, and we again emphasize that they are an output of the model and not an input. The dashed curves in Figure 3A show the Slip law predictions for these velocity steps, using these parameter values. The Slip law predicts the behavior of the granular model quite well, excluding the initial rounding that occurs over a slip distance of up to $\sim D_{mean}$ in the simulations. For the 4-order velocity jump to 2 m/s there is some contribution to the measured shear stress from bulk inertia of the gouge; however, this contribution is expected to be small for slip distances larger than a modest fraction of D_{mean}, and should not influence the Slip law fit to the data (Appendix B).

Figure 3B shows the variation of gouge thickness with slip distance (dashed lines) in comparison to the variation of friction coefficient, for the same velocity steps in panel A. The simulations show that the gouge layer approaches its future steady state thickness H_{ss} over a slip distance comparable to the slip distance for the evolution of friction (the gouge dilates with slip, but we plot $H_{ss} - H$ for easier comparison to the friction data). The good correlation between gouge thickness and friction (and hence log[state]), and the accepted parallels between state and gouge thickness (i.e., that the mushrooming of asperities that increases contact area also brings the surfaces closer together (Sleep, 1997)), make it natural to ask whether variations in gouge thickness are a useful proxy for variations in state.

Figure 4A shows results for similar simulations with an initial steady-state load-point velocity of 10^{-2} m/s, and velocity steps of up to $+2$ and -3 orders of magnitude. These show that friction evolves to its new steady state over a slip distance that is independent of the sign as well as the magnitude of the velocity step, again precisely the Slip-law description of state evolution. The variation of gouge thickness during these velocity steps is shown in Figure 4B, which indicates that the gouge thickness for velocity step increases evolves to its new steady state over a slip distance comparable to that for the evolution of stress, as in Figure 3B. In contrast, the gouge thickness during velocity step decreases evolves to its new steady state over a slip distance shorter than that observed for the friction coefficient in the same experiments, especially for the two- and three-order-of-magnitude step downs. This is emphasized by the gray curves in Figure 4B, which show the thickness evolution for the step velocity decreases, flipped and rescaled to cover the same range as the corresponding 1- and 2-order step increases (the total thickness change is larger for the step increases). This asymmetry of the transient response to changes in driving velocity, in conjunction with the symmetric response of the friction coefficient, indicates that gouge thickness is an incomplete description of state. Other aspects of the granular structure, such as force fabric and structural anisotropy, must contribute to the state of the system.

The prediction that gouge thickness evolves much more rapidly with slip in response to step velocity decreases than increases appears to be borne out by laboratory experiments (Figure 4C; see also Rathbun and Marone (2013, Figures 6-7) and Mair and Marone (1999, Figure 10a)), although a more systematic comparison to existing lab data is certainly warranted. In fact, the asymmetric response of the gouge thickness in the simulations is very reminiscent of the Aging law prediction for friction, especially the modified form of the Aging law that T. Li and Rubin (2017) argued was more faithful to the underlying concept of contact "age" (their Figure 5a). We will return to this point during the discussion of slide-hold simulations.

The single set of (Slip law) RSF parameters that best matches the velocity steps with $V_i = 10^{-2}$ m/s are determined from the simplex method to be $a = 0.024$, $b = 0.018$, and $D_c = 1.7D_{mean}$, very similar to the values determined previously for the step increases from $V_i = 2\times10^{-4}$ m/s. Laboratory investigations of the velocity-dependence of the RSF parameters show somewhat mixed results. For order-of-magnitude velocity steps on initially bare granite samples, B. D. Kilgore et al. (1993) found variations of a and b of no more than a few tens of percent for initial velocities ranging over 4 orders of magnitude. In contrast, similar experimental protocols conducted by Mair and Marone (1999) on synthetic fault gouge indicate that D_c increases systematically by up to 2 orders of magnitude, and that (for sample slip distances exceeding ∼15 mm) a decreases systematically by a factor of 2–3, as the initial velocity increases over a range of 3 orders of magnitude. However, using similar starting materials, Bhattacharya et al. (2015) found that velocity step increases of 1 and 2 orders of magnitude from a single starting velocity, and step decreases of 1 and 2 orders of magnitude back to that same velocity, were fit extremely well by the Slip law with constant RSF parameters.

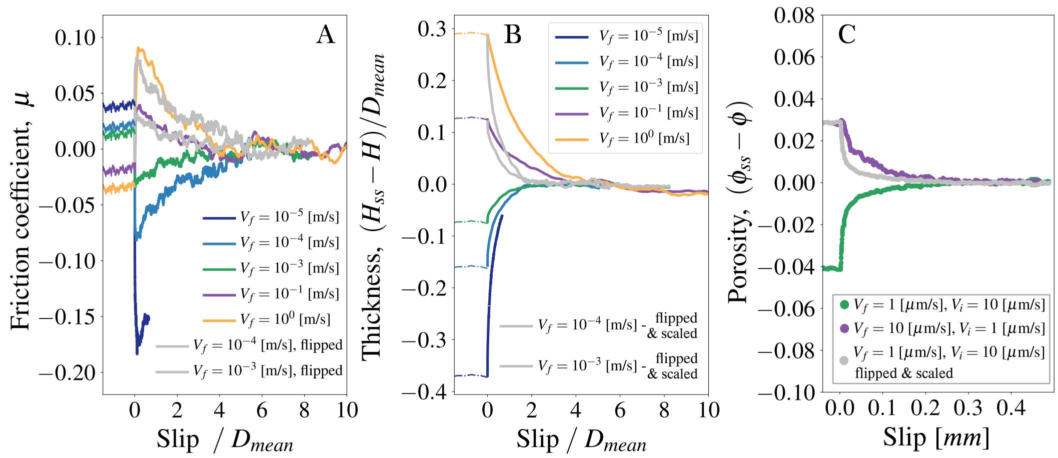

Figure 4. The variation of (A) friction coefficient and (B) gouge thickness, in simulations with velocity steps up to +2 and −3 orders of magnitude. The initial driving velocity in all tests is $V_i = 10^{-2}$ m/s. The simulation with $V_f = 10^{-5}$ m/s has yet to run to completion (the future steady state values are estimates only), but is sufficient to demonstrate that the thickness initially varies much more rapidly than stress. The gray curves in (A) are the step-down simulations, flipped to emphasize the stress symmetry between the step increases and decreases. The results in both panels are averaged over seven different realizations, with normal stress fixed at 5 MPa. (C) The variation of porosity in gouge experiments in response to ±1 order of magnitude increases and decreases in velocity from and back to the initial velocity of $V = 1$ μm/s. The experiments were performed by Marone et al. (1990, as reported by Segall and Rice, 1995) on water saturated but drained (∼constant pore pressure) layers of Ottawa sand. The gray curves in panels (B) and (C) are step-down simulations (B) and the lab experiment (C), flipped and scaled to the same initial value as the corresponding step up, to emphasize the much more rapid response (with respect to slip) of porosity (thickness) to the velocity step decreases.

5.2.1 The influence of confining pressure

In addition to velocity steps at a normal stress of $\sigma_n = 5$ MPa and initial velocities V_i of 10^{-2} and 2×10^{-4} m/s, we also conducted 1- to 3-order-of-magnitude velocity increases at $\sigma_n = 1$, 5 and 25 MPa at $V_i = 10^{-3}$ m/s. The results, shown in Figure 5, indicate that the magnitude of direct and evolution effects vary slightly but not systematically with σ_n. We again search for the single sets of (Slip law) parameters that best match all the velocity jumps at each confining pressure, using the simplex method (Table 2). Except for D_c being modestly larger at the largest σ_n, and a and b being larger at the smallest σ_n, the parameters seem to be largely independent of confining pressure.

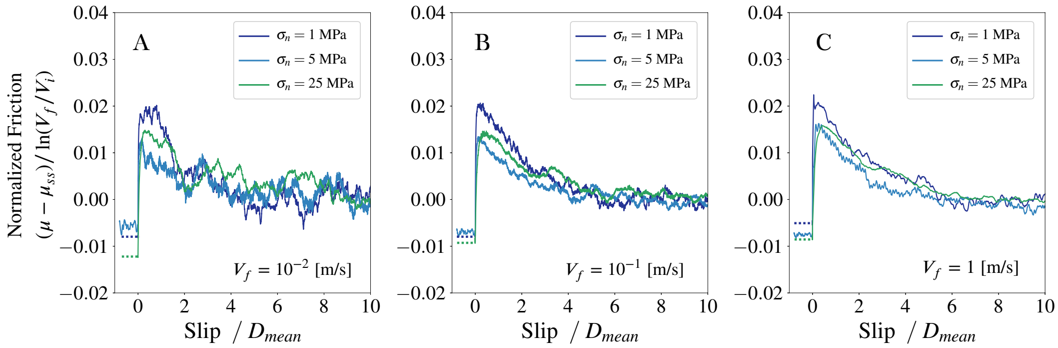

Figure 5. The variation of normalized friction coefficient, $(\mu - \mu_{ss})/\ln(V_f/V_i)$, for velocity step-ups of (A) one order, (B) two orders, and (C) three orders of magnitude, in systems with confining pressure $\sigma_n = 1, 5,$ and 25 MPa. With this normalization, rough estimates of a (the jump across the velocity step) and b (the amplitude of the decay following the peak) can be read directly from the vertical scale (the signal/noise ratio increases with the size of the velocity step). The initial driving velocity is $V_i = 10^{-3}$ m/s in all tests. The results are averaged over seven different realizations of the same imposed loading conditions.

Table 2. The RSF parameters obtained for velocity steps at $\sigma_n = 1,\ 5$ and 25 MPa and $V_i = 10^{-3}$ m/s.

Normal stress	RSF parameters			
σ_n	a	b	$a - b$	D_c/D_{mean}
1 MPa	0.0290	0.0226	0.0064	1.83
5 MPa	0.0202	0.0135	0.0067	1.92
25 MPa	0.0232	0.0145	0.0087	3.23

5.2.2 Critical slip distance or critical strain?

The critical slip distance in our default system velocity-step experiments is roughly 1.7 times the mean particle diameter D_{mean} (see Figs. 3-4). This seems reasonable, given that in laboratory fault friction experiments the critical slip distance D_c is often interpreted as being close to an asperity size (Marone, 1998b; J. H. Dieterich et al., 1981). However, laboratory data are somewhat ambiguous with regard to whether a critical strain or a critical slip distance controls the approach to a new frictional equilibrium. J. H. Dieterich et al. (1981) reported that the critical slip distance is largely independent of gouge thickness, an observation he interpreted as indicative of slip localization within the gouge (i.e., a critical strain over a layer thickness that was insensitive to gouge thickness). Marone and Kilgore (1993) reported that some gouges had a critical slip distance that increased quasi-linearly with gouge thickness (i.e., a critical strain), while others had a much weaker dependence upon thickness, possibly reflecting variable degrees of localization.

We have run step velocity increase simulations from $V_i = 10^{-2}$ m/s using the model that has twice the dimensions of the default model (although 1.8 times the thickness), with all other grain and system properties being identical to the default model. A comparison to the default model is shown in Figure 6. We find that the critical slip distance following velocity steps is 1.9 times as long in simulations with 1.8 times the model thickness (RSF parameters: $a = 0.028$, $b = 0.019$, and $D_c/D_{mean} = 3.3$, compared to $a = 0.024$, $b = 0.018$, and $D_c/D_{mean} = 1.7$ for the default model at $V_i = 10^{-2}$ m/s), suggesting that indeed it is a critical strain that governs the approach to the new steady state. As a result, rescaling the slip distance (x-axis) by the ratio of the model dimensions

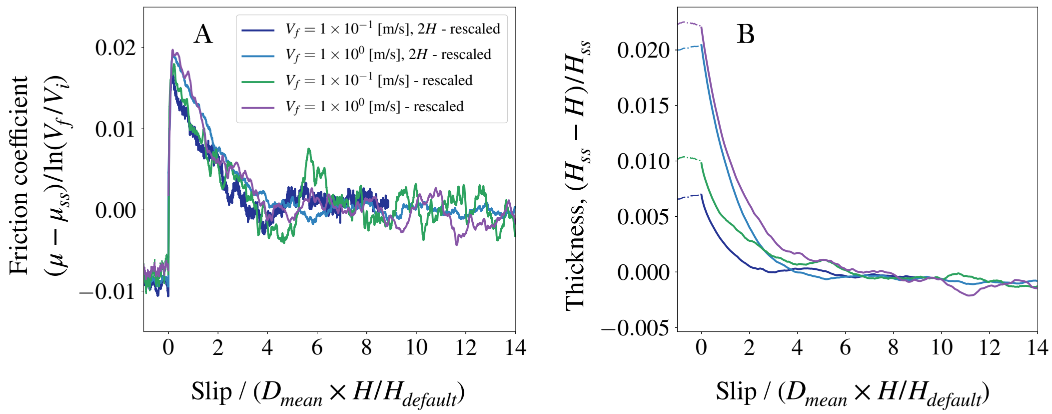

Figure 6. (A) The variation of normalized friction coefficient with normalized slip for velocity step-ups of $1-2$ orders of magnitude, in the default system and the system with twice the domain size. (B) The variation of the gouge thickness normalized by the initial gouge thickness for the same velocity steps in (A). In both panels, the slip distance (x-axis) is scaled by the ratio of the gouge thickness to the default gouge thickness $H_{default}$. $V_i = 10^{-2}$ m/s and $\sigma_n = 5$ MPa. The results are averaged over seven different realizations of the same imposed loading conditions.

shows that the frictional behavior for both systems almost collapses (with some noise) to a single curve. The critical strain, using $\gamma_{xz} = \partial u_x/\partial z + \partial u_z/\partial x = \partial u_x/\partial z$, is $\gamma_{xz_c} \sim D_c/H \sim 0.13$. In contrast, the gouge thickness curves, when normalized by their (future) steady-state values, do not completely collapse when plotted as a function of rescaled slip distance (Figure 6B). We obtained similar results (not shown here) for $V_i = 10^{-1}$ and 10^{-3} m/s.

5.2.3 The gouge dilation angle

Several authors have commented on the potentially important contribution of fault gouge dilatancy or compaction to the measured value of friction (Morrow & Byerlee, 1989; Morgan, 2004; Marone et al., 1990; Beeler & Tullis, 1997). Marone et al. (1990) proposed that the "apparent" friction, μ^A, defined as the ratio of the shear to normal stress τ/σ (what is measured in laboratory experiments and our numerical simulations), can be written

$$\frac{\tau}{\sigma} = \mu^A = \mu^f + \frac{d\delta_n}{d\delta_s}\,, \tag{16}$$

where $d\delta_n/d\delta_s$ is the instantaneous ratio of fault-normal displacement δ_n to slip δ_s (dilation taken to be positive and compaction negative here), and μ^f can be considered to be some hypothetical "intrinsic" friction that would be measured in the absence of fault-normal displacements.

Changes in $d\delta_n/d\delta_s$ in lab experiments are often larger than changes in the observed friction μ^A. Because of this, Beeler and Tullis (1997) pointed out that if μ^f is thought to be given by equation (1), the direct effect parameter a would have to be negative; i.e., at constant state, materials would have to weaken with increasing slip speed. As this violates standard interpretations of the source of the direct effect, they argued that μ^f should be interpreted not as resulting from the total energy dissipated in the fault zone, but as only the energy dissipated in fault-parallel shear. They showed that with this definition of μ^f, the time-dependent plastic contribution to $d\delta_n/d\delta_s$ should be neglected in equation (16).

For granular models we are not persuaded that it is useful to speak of an "intrinsic" friction that is distinct from the contribution of dilatancy to the measured μ^A. And, as a practical matter, it

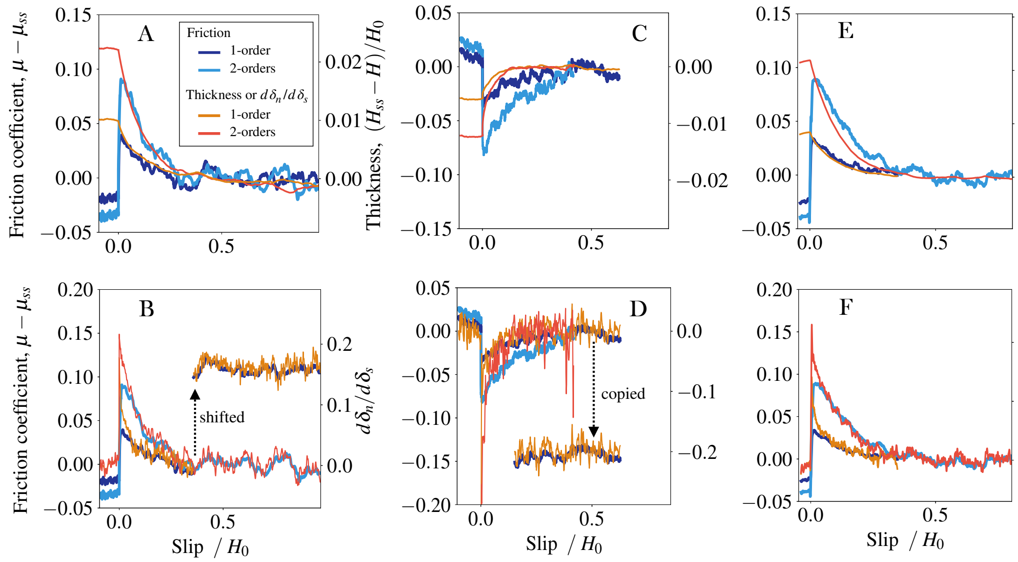

Figure 7. (A-C-E) The variation of frictional resistance and normalized gouge thickness with slip distance in velocity step tests. Slip here is normalized by the nominal gouge thickness H_0, so the horizontal axis is the nominal shear strain. (A): The default model with step increases of 1 and 2 orders of magnitude. (C): The default model with step decreases of 1 and 2 orders of magnitude. (E): Step increases of 1 and 2 orders of magnitude in the system with twice the dimensions of the default model. The thickness change in these panels is normalized by H_0, so the vertical axis is the nominal dilational strain, but the scale factor relating the normalized thickness and friction axes in each panel is the same as in Figure 4. (D-B-F) The variation of friction and normal to shear deformation rate with respect to normalized slip distance for the same experiments shown in the panels immediately above. The ratio between the $d\delta_n/d\delta_s$ and friction scales (1.44) is the same in all panels. The $d\delta_n/d\delta_s$ minima in panel (D) are at -0.25 and -1.38 (the latter off scale) for the 1- and 2-order step decreases, respectively. All experiments are performed at $\sigma_n = 5$ MPa and $V_i = 10^{-2}$ m/s; H_0 is taken to be the value of H_{ss} under these conditions. The results are averaged over seven different realizations of the same imposed loading conditions.

is not trivial to separate $d\delta_n/d\delta_s$ as observed in laboratory experiments into time-dependent plastic and slip-dependent geometric components, as advocated by Beeler and Tullis (1997). Nonetheless, our measurements of $d\delta_n/d\delta_s$ can be compared to both laboratory experiments and our measured μ^A. Figure 7 shows the evolution of friction, the gouge layer thickness, and $d\delta_n/d\delta_s$, for 1- and 2-order-of-magnitude velocity step increases and decreases for our default model, as well as 1- and 2-order-of-magnitude step increases for the model with dimensions twice as large. The scale factor between friction and thickness changes in panels A, C, and E is the same as in Figures 3, 4, and 6. As in those figures, there is a reasonably close correlation between the measured friction and gouge thickness for the step increases but not the step decreases. However, the correlation between the measured friction and $d\delta_n/d\delta_s$ for the step increases, as well as for the step decreases once the system is close to steady state, is even more striking. Note the difference in scale; the variation in $d\delta_n/d\delta_s$ is about 40–50% larger than the variation in μ^A. In steady-sliding laboratory experiments on 2-D glass rods, Frye and Marone (2002) found a ratio closer to 1. Hazzard and Mair (2003) also found a ratio of ~ 1 at steady state for both 2-D and 3-D granular simulations with Hertzian grain-grain interactions.

Our granular simulations show that upon a step increase in velocity, the maximum value of $d\delta_n/d\delta_s$ exceeds the direct-effect friction change $\Delta\mu_{\text{direct}}$ by anywhere from a few tens of percent to a factor of about two (Figures 7B and 7F). The difference is larger in our simulated velocity-step decreases; because of the more rapid evolution of thickness with slip, $d\delta_n/d\delta_s$ following the velocity step exceeds $\Delta\mu_{\text{direct}}$ by more than a factor of 5 for the 1-order step down and more than a factor of 10 for the 2-order step down (Figure 7D). These results are within the ballpark of laboratory values. In experiments on synthetic gouge in a triaxial shear apparatus, Marone et al. (1990, figures 20-21) find that $d\delta_n/d\delta_s$ exceeds $\Delta\mu_{\text{direct}}$ by a factor of 4–6, independent of the magnitude of the velocity step, for both step increases and the one step decrease shown. Using data from the same paper, however, and plotting thickness as a function of slip, Segall and Rice (1995) show an example (reproduced here as Figure 4C) for which $d\delta_n/d\delta_s$ is significantly larger for the step down than the step up. Similarly, Mair and Marone (1999, figure 10a) show thickness vs. slip for a 1-order velocity step increase and decrease in a double-direct shear experiment on synthetic gouge where $(d\delta_n/d\delta_s)/\Delta\mu_{\text{direct}}$ is about 2.5 for the step increase, but many times larger for the step decrease (for the step increase $(d\delta_n/d\delta_s)/\Delta\mu_{\text{direct}} \sim 0.03/0.005\ln[10]$, where 0.005 is the value of a for $\sigma_n = 25$ MPa, total slip 18–20 mm, and $V = 1$ to 10 mm/s in their figure 8a). Using a rotary shear apparatus, Beeler and Tullis (1997) present data from 1-order velocity step decreases where $d\delta_n/d\delta_s$ exceeds $\Delta\mu_{\text{direct}}$ by a few tens of percent for initially intact granite that develops a gouge layer through wear, and by a factor of about 2.5 for synthetic granite gouge. This is an area where a more thorough comparison between the granular gouge simulations and existing laboratory data is certainly warranted.

As a final investigation of equation (16), we ran velocity-step simulations while enforcing a constant volume (gouge thickness) boundary condition ($d\delta_n/d\delta_s = 0$, so $\mu^A = \mu^f$). For a step increase this entails a transient increase in normal stress, as the gouge, which dilates at constant normal stress, is prevented from doing so. Remarkably, the transient friction response in the constant-volume simulations is indistinguishable from that in the corresponding constant-normal-stress simulations (Figure 8). We are thus faced with the surprising observation that at constant normal stress there is a very close correlation between $d\delta_n/d\delta_s$ and μ^A for most of the friction evolution after the step velocity increases in Figs. 7B and 7F, seemingly consistent with the spirit of equation (16), while essentially identical friction evolution occurs in simulations in which $d\delta_n/d\delta_s$ is forced to be zero.

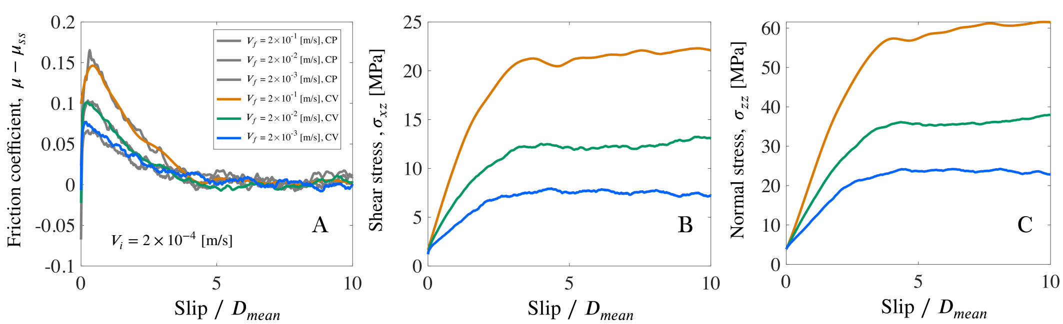

Figure 8. Results from constant-volume velocity-step experiments. (A) shows the variation of friction; (B) and (C) show the variation of shear and normal stress applied by gouge grains to the driving plate, as functions of slip distance. All experiments use the default model with an initial normal stress of 5 MPa and $V_i = 2\times10^{-4}$ m/s. Gray lines in (A) show the frictional behavior for the corresponding constant normal stress experiments. The results are averaged over seven different realizations of the same imposed sliding conditions.

5.2.4 Is there localization in the granular gouge layer?

A plot of the particle velocity through the gouge, $u_x(z)$, spatially averaged over x and y and temporally averaged over an upper plate displacement of $0.1D_{mean}$, is shown in Figure 9A for a steady-state shearing simulation performed at the load-point velocity $V_{lp} = 10^{-2}$ m/s. The steady-sliding velocity profile decays linearly away from the shearing plate, and shows no sign of localization. Following an order of magnitude velocity-step increase, we further measure the velocity variation with distance from the driving plate during the first 0.001 D_{mean}, 0.01 D_{mean} and 0.1 D_{mean} shearing distance. The results are plotted in Figures 9B-D and show no signs of strain localization immediately or shortly after the velocity step (in Figure 9B the shear wave generated by the velocity step at the upper pate has yet to reach the bottom plate; see Appendix B). Hatano (2015) suggested that the duration of the friction transient following his simulated velocity steps might correspond to the slip distance required for the gouge to approach its new steady state velocity profile, but as this occurs over distances $< 0.1D_{mean}$ in Figure 9, compared to slip distances of several D_{mean} for the friction transient, this is clearly not the case in our simulations.

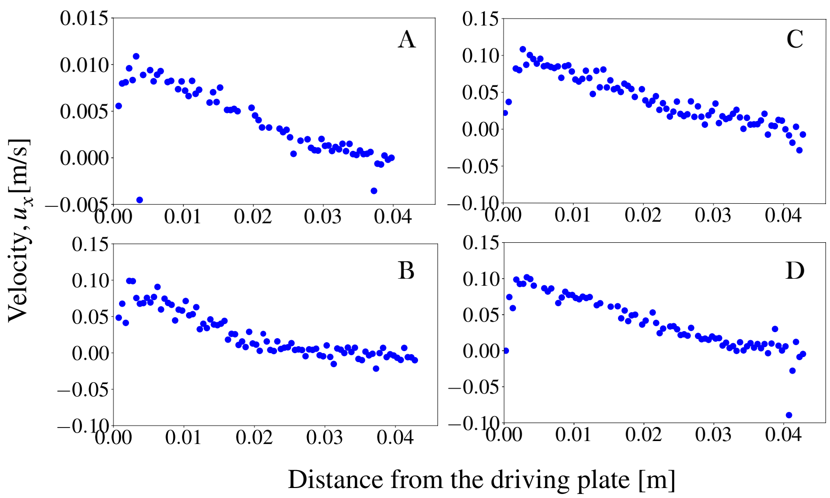

Figure 9. The velocity profile of the granular gouge in the default system. The driving velocity is initially $V_i = 10^{-2}$ m/s, as in Figure 4. Panel (A) shows the velocity profile at steady sliding with velocity V_i, measured over a slip distance 0.1 D_{mean}. Panels (B), (C) and (D) show the velocity profiles measured in the first 0.001 D_{mean}, 0.01 D_{mean}, and 0.1 D_{mean}, respectively, following an order of magnitude step velocity increase. In (B), the shear wave generated by the velocity jump at the upper plate just 3×10^{-5} s earlier has traversed only about half the gouge thickness (see Appendix B). The normal stress is fixed at 5 MPa. The indicated velocity is a spatial average over the x and y directions.

The absence of localization in our system is also consistent with the adopted dimensionless pressure ($\bar{P}_{\text{Hertz}} = [P/E]^{2/3} \sim 2 \times 10^{-3}$ for $\sigma_n = 5$ MPa), which puts it near the stiff or rigid grain limit. The studies by de Coulomb et al. (2017) and Bouzid et al. (2015) show that in our range of packing pressure and inertial numbers, systems do not show persistent localized deformation, although Aharonov and Sparks (2002) report periods of spontaneous transient slip localization in 2-D simulations with $\bar{P}_{\text{Hook}} = 10^{-3}$. In contrast, persistent patterns of localized deformation in the form of simple shear bands are expected in systems that operate in the soft grain regime ($\bar{P} \gg 10^{-3}$) (de Coulomb et al., 2017; Le Bouil et al., 2014; Amon et al., 2012; Darnige et al., 2011). In laboratory experiments on synthetic gouge (Sleep et al., 2000), and gouge formed by wear of initially intact rock (Beeler et al., 1996), slip appears to be localized, but this may be associated with processes such as grain breakage that are not included in our model (see Abe and Mair (2009) for a granular simulation that includes breakage at the grain scale, and Aghababaei et al. (2018) for atomistic simulations that include asperity breakage and wear at the atomic scale).

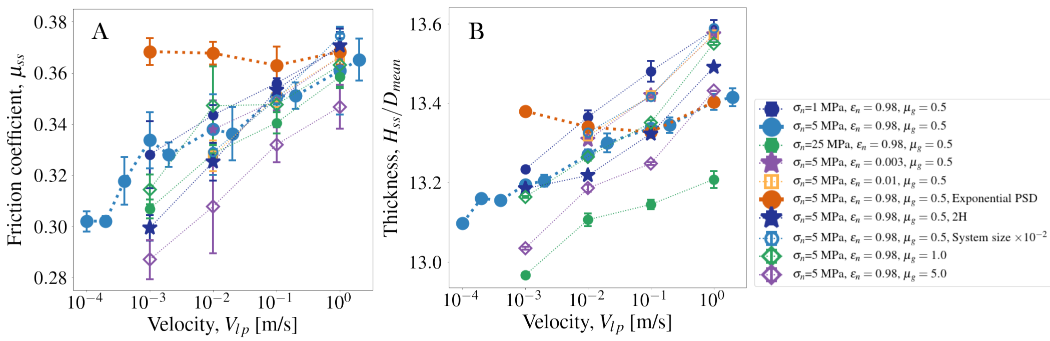

Figure 10. (A) The variation of steady-state friction coefficient with driving velocity in the default system at three different normal stresses, and in systems with different values of the grain-grain friction coefficient, restitution coefficient, size (smaller by 100x), ratio of steady-state gouge thickness H_{ss} to mean particle diameter D_{mean} (1.8× larger), and grain size distribution (quasi-exponential). (B) The variation of H_{ss}/D_{mean} for the simulations in (A). For models that have a different number of grains per unit area ($L_x \times L_y$) than the default model, the ratio H_{ss}/D_{mean} has been further normalized by the ratio of that number to the number of grains per unit area in the default model (a correction that is $\leq 10\%$ for the models with the same L_x and L_y). This normalization is performed for the systems with quasi-exponential grain size distribution, with 1.8 times the H_{ss}/D_{mean} of the default model (2H), and with different restitution coefficients and grain-grain friction coefficients. Error bars indicate one standard deviation of all friction measurements over a sliding distance of $5D$ for each of seven different realizations (initial grain arrangements). Most error bars in (B) are smaller than the symbol size.

5.2.5 The influences of grain-grain friction coefficient, restitution coefficient, and grain size

To explore the generality of our observations and which grain-scale properties may influence the results, we investigated the steady-state behavior, and the transient response to velocity-steps, of systems with different grain-grain friction coefficients, grain-grain restitution coefficients, and (while keeping the ratio of gouge thickness to grain size fixed) grain size. Figure 10 shows the variation of the steady-state friction coefficient (A) and gouge thickness (B) with driving velocity for the default system and for systems with different grain properties. The variation of steady-state friction with driving velocity is somewhat sensitive to the details of the system, although frictional behavior remains velocity-strengthening for all cases with mean slopes of $0.005 \lesssim (a-b) \lesssim 0.007$. The variation of gouge thickness with velocity shows that the gouge layer remains logarithmically dilatant, with similar normalized dilation rates of roughly $0.01 D_{mean}$ per decade, corresponding to normal strains of order 10^{-3} per decade, for all systems.

Note that increasing the grain-grain friction coefficient decreases the macroscopic friction slightly, consistent with previous studies (Silbert, 2010), presumably as a result of enhanced grain rolling. From dimensional analysis, decreasing the grain and system sizes by the same scale factor is not expected to lead to differences in macroscopic behavior, as this changes only the magnitude of the gravitational stress relative to the confining pressure, which is already extremely low (Appendix A). Comparing the default model to the system reduced in scale by a factor of 100 in Figure 10 shows that this is generally the case, to within the scatter of the data.

The choice of restitution coefficient ϵ also has very little influence on frictional behavior. Figure 10A shows that values of ϵ_n ranging from nearly fully damped (0.003 and 0.01) to near-zero damlping (the default value of 0.98) show essentially the same value of μ_{ss} as a function of velocity. Previous numerical studies have also demonstrated that for inertial numbers $I_n \lesssim 10^{-2}$, varying the grain-grain damping exerts almost no influence on the steady-state frictional behavior of the system

(MiDi, 2004) (this is unlike the behavior at higher I_n, where increasing the damping during grain-grain collisions decreases the rate of velocity strengthening and dilation with increasing driving velocity and inertial number (Silbert et al., 2001; MiDi, 2004)).

The influence of these grain-scale properties on the transient frictional response to velocity-step tests were also very modest. Although we have not formally fit the results to determine the RSF parameters a, b, and D_c, directly comparing the transient responses to those for the default model generally show differences that are within or near the apparent noise level (Supplementary Figures S3, S5, and S6).

5.2.6 The influence of grain size distribution

Unlike the grain-scale properties of the previous section, we find that grain size distribution has a dramatic influence on the macroscopic behavior of the system. We have run simulations with a quasi-exponential grain size distribution, which better represents actual fault gouge (Marone & Scholz, 1989; Sammis & King, 2007; Billi, 2005; An & Sammis, 1994).For the quasi-exponential size distribution, we targeted generating a distribution with grain sizes ranging from 0.5 to 5 mm, with D_{mean} = 1.5 mm, and distribution form PDF$(D) = \lambda^{-1} \exp[-(D - \mathcal{M})/\lambda]$, with distribution parameters $\mathcal{M}$ = 1 mm and λ = 2 mm. The resulting system, generated by a random particle generation algorithm in LAMMPS, has D_{min} = 0.5 mm, D_{max} = 4.9 mm, and D_{mean} = 1.5 mm. We reduced D_{mean} by half, relative to the default system, to ensure that the largest particle size was no larger than the 5-mm particles in the bounding rigid blocks (larger gouge particles led to a roughly 5-mm periodicity in friction during quasi-steady sliding). We also found that the exponential distribution led to apparently noisier (more variable) friction during steady sliding; on the assumption that a longer model dimension in the sliding direction would reduce the influence of individual force chains, the quasi-exponential system was given dimensions $L_x = 4L_y = 6L_z = 160\ D_{mean}$ (Figure 11). This reduced the apparent noise substantially. A few simulations of the same dimension using the quasi-normal grain size distribution verified that increasing L_x/L_z from 1.5 to 6.0 didn't change the steady-state friction level, its dependence upon slip speed, the rate of change of gouge thickness with shear velocity, or the qualitative behavior of the system during velocity-stepping or slide-hold protocols.

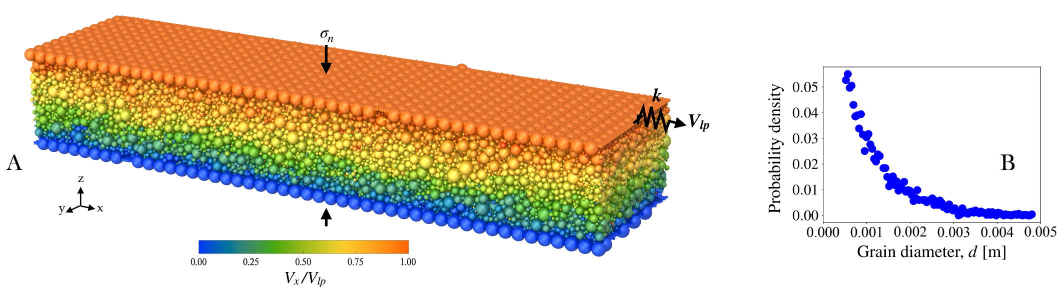

Figure 11. (A) Visualization of the virtual rock gouge experiment with the quasi-exponential grain size distribution, with mean grain diameter D_{mean} = 1.5 mm. Colors show the velocity of each grain in the x direction, averaged over an upper-plate sliding distance of D_{mean}. The driving velocity is V_{lp} = 0.1 m/s. (B) The size distribution of grains in the gouge layer.

The variation, with driving velocity, of the steady-state friction coefficient and gouge thickness for the quasi-exponential grain size distribution are shown by the solid orange symbols in Figs. 10A and B, respectively. Given the error bars in panel A, one could perhaps argue that the system is velocity-neutral. However, because the gouge thickness, which has much smaller uncertainties, decreases as V_{lp} increases from 10^{-3} to 10^{-1} m/s, and increases from 10^{-1} to 1 m/s, we think it is more likely that the system is steady-state velocity strengthening as the shear velocity increases from $V_{lp} = 10^{-1}$ to 1 m/s, and nearly velocity-neutral or slightly velocity-weakening as

V_{lp} increases from 10^{-3} to 10^{-1} m/s (an association between steady-state velocity-weakening and gouge-thinning, and steady-state velocity-strengthening and gouge-thickening, underlies recent versions of STZ theory (Lieou et al., 2017)). Therefore the gouge thickness, and perhaps the friction coefficient, vary non-monotonically with driving velocity. DeGiuli and Wyart (2017) previously observed a non-monotonic variation of friction coefficient with shear velocity in 2-D granular simulations and in the range of $\bar{P}$ and inertial numbers we have explored. The grain size distribution used in their model is not specified. The non-monotonic variation of friction coefficient has also been observed in several experimental granular physics studies, including those by Dijksman et al. (2011), G. H. Wortel et al. (2014), and G. Wortel et al. (2016). However, it is not straightforward to separate the potential contributions of time-dependent contact-scale processes from purely granular rearrangements in those experiments. van der Elst et al. (2012) also observed a non-monotonic variation of gouge thickness with shear rate in experiments using angular grain shapes, while experiments using spherical grains showed a monotonic increase of gouge thickness with shear rate. The friction coefficient, and the influence of grain size distribution on the velocity-dependence of gouge thickness, were not explored in their study.

We also performed a limited number of velocity-step simulations using the quasi-exponential grain size distribution. The results are shown in Supplementary Figure S7. They include a subset of 1- and 2-order-of-magnitude velocity steps up or down from initial driving velocities of 10^{-2}, 10^{-1}, and 1 m/s. Owing to the large model size we averaged only 3 realizations of each set of conditions, and the results are much noisier than for our normal distribution simulations (although less noisy than the average of 7 realizations of the exponential distribution using the default simulation size). All of these tests show a direct velocity effect and an opposing state evolution effect, with $a \sim 0.0085$ for the step with the highest signal/noise ratio (a 2-order step down; Supplementary Figure S7-C), and values not far from this for the others. This is within the range typically reported for laboratory experiments (e.g., Mair & Marone, 1999).

The variation of gouge thickness following step velocity changes between 0.1 and 1 m/s, where steady-state friction and gouge thickness increase with slip speed, is similar to the behavior of models with a quasi-normal grain size distribution, in that the thickness monotonically approaches its future steady-state value at a decaying rate. However, for steps between velocities in the range of 10^{-3} to 10^{-1} m/s, where steady-state thickness (and perhaps friction) decrease with increasing slip speed, the transient thickness change becomes nonmonotonic. Following a velocity step decrease, for example, the gouge initially compacts, as for the quasi-normal grain size distribution, but then dilates by a greater amount to reach the new steady-state thickness. Where the signal-to-noise ratio is sufficient (e.g., Supplementary Figures S7-B and C, and to a lesser extent E and F), this transition from compaction to dilation seems to occur while the friction is monotonically (except for the noise) approaching its new steady state. The reverse behavior is seen for velocity step increases. We do not yet understand the origins of this behavior, and see no dramatic changes in the particle velocity profiles over the course of the non-monotonic thickness changes. The change in sign of $\delta d_n/\delta d_s$ at these lower velocities, together with the monotonic nature of the (smoothed) friction (and hence state) transient, is inconsistent with the notion that state and porosity are linked in any simple way. Considering only the steady-state thickness changes (Figure 10B), the positive direct velocity effect (a stress increase for a velocity increase) is also inconsistent with the simple notion that the direct effect comes from sliding at the new velocity but the old porosity. However, this positive direct effect is consistent with the initial thickness change following a velocity step having the opposite sign than the steady-state thickness change (e.g., an initial thickness increase for a step velocity increase).

We ran one slide-hold simulation using the quasi-exponential grain size distribution, with initial sliding velocity $V_i = 0.1$ m/s. It showed logarithmic-with-time stress relaxation and gouge compaction, with a compaction rate of about half that of the model with a quasi-normal grain size distribution, after normalizing by the different initial gouge thicknesses. Again considering only steady-state thickness changes in Figure 10B, this result seems inconsistent with the intuitive statement that the effect on gouge thickness of an order-of-magnitude increase in hold time is roughy comparable to the effect of an order-of-magnitude decrease in slip speed (Figure 2). And, as with the positive value of the direct velocity effect, the compaction during the hold seems qualitatively consistent with the initial compaction following a step velocity decrease for the quasi-exponential grain size distribution; however, the subsequent dilation following the velocity step remains unexplained.

5.3 Slide-hold simulations

The main emphasis of this paper has been granular simulations of velocity-step experiments, which have long been known to be well-modeled by the RSF framework using the Slip law for state evolution (A. Ruina, 1983; Bhattacharya et al., 2015). We have shown that the granular simulations, like the Slip law, predict that following the initial direct velocity response, friction decays quasi-exponentially to its new steady state over a slip distance that is independent of the magnitude and sign of the velocity step. Moreover, with apparently no important free parameters, the granular model with our adopted quasi-normal grain size distribution produces a direct velocity effect and a subsequent state evolution effect with amplitudes that vary linearly with the logarithm of the velocity jump, with values of the RSF parameters a and b that are reasonably close to those determined empirically in the laboratory. Changing to our quasi-exponential grain size distribution changes only the magnitudes of a and b, while still leaving them close to lab values (and perhaps introducing enough velocity dependence to make the system transition from steady-state velocity weakening to velocity strengthening with increasing slip speed).

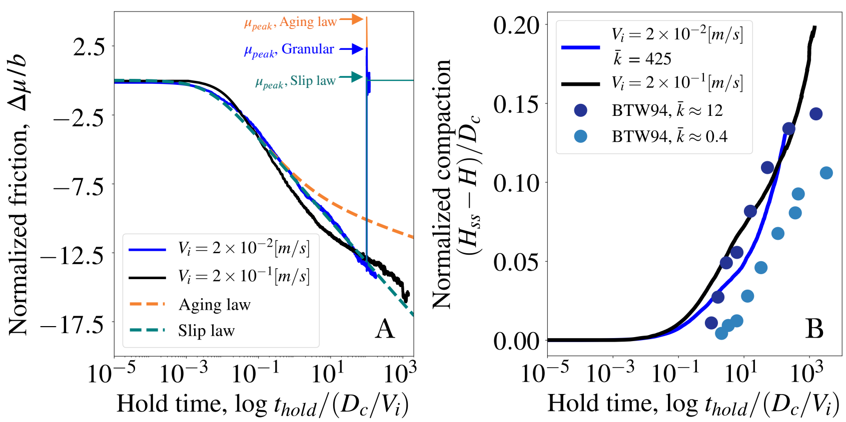

Figure 12. (A) The blue and black lines show the variation of friction coefficient, normalized by the RSF parameter b, as a function of normalized hold time, for granular slide-hold simulations with prior driving velocities V_i of 2×10^{-2} (blue) and 2×10^{-1} (black) m/s. The orange and green dashed lines show the predictions of the Slip and Aging laws, respectively, using the RSF parameters determined from the velocity step tests in Figure 4. This panel also shows (in blue) results of a reslide at $V = V_i = 2 \times 10^{-2}$ m/s following a normalized hold time $t_{hold}/(D_c/V_i)$ of 100, in comparison to the the Aging and Slip law predictions. The peak friction upon reslide is indicated by μ_{peak}. The confining pressure in all simulations is 5 MPa, and the dimensionless stiffness $\bar{k} \equiv k_{\text{eff}}D_c/(b\sigma) \approx 425$. (B) Blue and black lines show the change in gouge thickness during the slide-hold granular simulations of panel (A). (solid dots) The change in gouge thickness during hold experiments on granite reported by Beeler et al. (1994), who used two different (low and high) machine stiffnesses. An estimated slip-weakening distance $D_c \approx 3\mu$m is used to normalize results from the laboratory experiments. Both low and high stiffness laboratory experiments were performed at 25 MPa confining pressure.

In this section, we present preliminary results from the default granular model using loading conditions intended to simulate slide-hold protocols. We focus on both the stress decay during the hold and the corresponding change in thickness of the gouge layer. Laboratory observations indicate that in response to an imposed load-point hold, the stress decays in a manner consistent with the Slip law and not the Aging law, which exhibits too little decay due to time-dependent healing (Bhattacharya et al., 2017). Furthermore, during the hold the gouge undergoes fault-normal compaction roughly as the logarithm of time. Although RSF classically makes no explicit prediction about fault-normal displacements, the conventional interpretation of log-time fault-normal compaction during holds is that it is consistent with the Aging law for state evolution. That is, compaction is viewed as going hand-in-hand with the plastic deformation of microscopic asperity contacts and log-time increase in true contact area under high local normal stresses (Berthoud et al., 1999; Sleep, 2006). This compaction is observed despite the fact that log-time healing as embodied by the Aging law for state evolution is ruled out by the stress data from the same slide-hold experiments.

We have thus far examined slide-hold simulations performed at two initial sliding velocities and $\sigma_n = 5$ MPa. Figure 12A shows the variation of normalized friction with normalized hold time for these tests, with the initial velocities of $V_i = 2 \times 10^{-2}$ m/s and 10^{-1} m/s shown by the blue and black curves, respectively. For standard RSF (equations 1–3 with constant parameter values), these curves would plot on top of one another when normalized in this fashion, a result that follows from dimensional analysis. Although the stress decay for the black curve ($V_i = 2{\times}10^{-1}$ m/s) is not strictly log-linear, a log-linear fit to that curve would be similar to the curve for $V_i = 2{\times}10^{-2}$ m/s. The figure also includes the predictions of the Aging and Slip laws, shown by the dashed orange and green lines, respectively, using the RSF parameter values determined independently from Slip law fits to the numerical velocity step tests. As described in the Computational Model section, for the RSF predictions we use a shear modulus of 300 MPa, leading to a normalized stiffness $\bar{k} = k_{\text{eff}} D_c/(b\sigma)$ of 425. For a velocity-strengthening system with such a large stiffness, increasing (decreasing) $\bar{k}$ by a factor of 2 shifts the Slip law fit left (right) by a slightly larger factor, but does not change the slope at long hold times (Bhattacharya et al., 2017, Appendix C2). The comparison between the blue and dashed green curves shows good agreement between the granular model and the Slip law prediction, as for the laboratory experiments of Beeler et al. (1994) analyzed by Bhattacharya et al. (2017). And the Aging law underestimates the stress decay during the holds, for the same reason that it underestimates the stress decay during lab experiments. This initial result suggests that the granular model, like the empirical Slip law, may capture much of the phenomenology of laboratory slide-hold tests. Further testing of the granular model over a broader range of slide/reslide velocities and spring stiffnesses, for comparison to available lab data, are currently underway.

In addition to seeming to match the stress decay during laboratory holds, the granular model qualitatively reproduces the observed reduction in gouge thickness with log hold time (Figure 12B). In the conventional RSF framework, because the stress data are well modeled by the Slip law with its lack of state evolution, the gouge would not be expected to compact. The paradox that it does so was also noted by Bhattacharya et al. (2017) in their analysis of the Beeler et al. (1994) slide-hold experiments. In contrast, and in agreement with laboratory experiments, our granular simulations show that log-time compaction during holds is present even though log-time healing as embodied by the Aging law is lacking. This behavior is reminiscent of the symmetric stress change/asymmetric thickness change in response to velocity step tests in Figure 4 (much more rapid variation in thickness than stress, following a step velocity decrease), and is another indication that equating state and porosity (Sleep, 2006; Lieou et al., 2017) neglects some fundamental aspect of granular friction.

5.3.1 Slide-hold-slide simulations

During both laboratory and simulated slide-hold-slide experiments, friction (shear stress) relaxes during the hold, but upon the reslide overshoots its future steady-state value by an amount $\Delta\mu_{peak}$, reflecting the ‘healing’ (strengthening at a reference slip speed) of the gouge during the hold. As shown by Bhattacharya et al. (2017), neither the Aging law nor the Slip law can successfully model, with a single set of parameter values, both the stress relaxation and the subsequent $\Delta\mu_{peak}$ for each of the high and low stiffness slide-hold-slide laboratory experiments of Beeler et al. (1994). In particular, although the Slip law can match the stress decay during holds for both stiffnesses moderately well, the predicted $\Delta\mu_{peak}$ for the high stiffness set-up is far too low to match the lab data (figure 8a of Bhattacharya et al., 2017). The reason is that for the high-stiffness set-up, the slip during the load-point hold is too low for the Slip law to allow significant healing.

Figure 12A shows the predicted $\Delta\mu_{peak}$ for the granular simulation (blue), Aging law (orange) and Slip law (green), the latter two using the same values of a, b, and D_c used to model the holds. Note that the Slip law predicts $\Delta\mu_{peak} \sim 0$, because almost no slip accumulates during the load-point hold, and that $\Delta\mu_{peak}$ from the granular simulation is much higher. This is the first sliding protocol we have modeled for which the stress history from the granular simulation differs qualitatively from that of the Slip law, and it differs (1) in the sliding protocol for which the Slip law most obviously fails to match lab data (the reslides following holds); and (2) in the proper sense to match the lab data better than the Slip law.

5.4 Exploring the microphysics of granular rate-state friction

There is currently no well-accepted explanation for the empirical, but moderately successful, Slip law for describing the rate- and state-dependent frictional behavior of rock and gouge. The only heuristic explanation of which we are aware is that of Sleep (2006), who proposed that it results from the highly nonlinear stress-strain relation at contacting asperities (e.g., that the modestly smaller stress following a velocity step decrease results in an exponentially smaller strain rate, and a symmetric stress response to step increases and decreases when plotted against slip). In this paper we have presented a physical model that, despite lacking meaningful time-dependence at the contact scale, reproduces the Slip law where that law matches experimental data well (velocity-step and slide-hold protocols), and may outperform the Slip law where that law does not work (the reslides following holds). We would therefore like to use the output of the granular model to understand the source of its lab-like (and RSF-like) behavior.

As a first step, we consider the source of the rate-dependence of granular friction. We expect that the log-time densification and relaxation of stress during holds (and by extension the densification with decreasing slip speed during steady sliding) is due to a reduction of elastic potential energy associated with local grain rearrangements. These rearrangements generate seismic waves that perturb nearby grains which might themselves be near the threshold for hopping, at a rate that decays quasi-logarithmically with time, as the driving stress and the opportunities for continued compaction lessen. This picture of grains as always vibrating, being perturbed by neighbors, and occasionally overcoming activation energy barriers, is conceptually similar to the traditional atomistic-scale view that the logarithmic rate-dependence in RSF (the $\log V/V_*$ term in Eq. 1) arises from a thermally-activated Arrhenius process (Rice et al., 2001; Lapusta et al., 2000; Chester, 1994). In that microscopic picture, the slip rate is $V = V_1 \exp(-E/(k_B T))$, where the product of the Boltzmann constant, k_B, and the temperature, T, is a measure of the average kinetic energy (KE) of the atoms. The activation energy E has the form $E = E_1 - P\Omega_A$, where P is a representative pressure and Ω_A is the associated activation volume. In this equation, V_1 can be interpreted as an attempt frequency times a slip displacement per successful attempt. Such an interpretation reproduces the empirical logarithmic form of the direct velocity dependence of friction with

$$a = \frac{k_B T}{P\Omega_A} \,. \tag{17}$$

A histogram of the KE (E_k) of every grain in a steady-state granular simulation with $V_{lp} = 2 \times 10^{-2}$ m/s is plotted on log-linear and log-log axes in Figs. 13A and B, respectively. Assuming that this KE plays the role of $k_B T$ in equation (17), we can use this measurement (mean value $\sim 2 \times 10^{-5}$ J/grain) to estimate a. We take the product of pressure and activation volume to be given by the elastic strain energy of grain compression, leading to

$$P\Omega_A \approx C \int_0^{\Delta_{ij}} F_n \, d(\delta_{ij}) = \frac{2}{5} C P d^3 \left[3(1-\nu^2) \frac{P}{E} \right]^{2/3} , \tag{18}$$

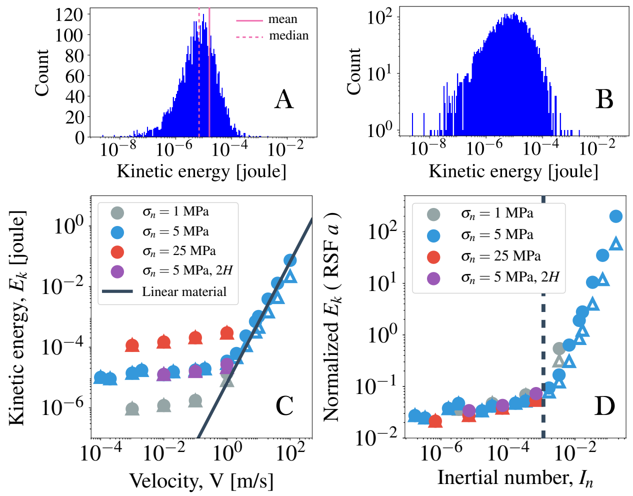

Figure 13. (A-B) Histograms of the per-grain KE during steady sliding at $V_{lp} = 2 \times 10^{-2}$ m/s in (A) log-linear (x-y) axes and (B) log-log axes. (C) The variation of the mean per grain KE (E_k) for steady-sliding simulations at a range of shearing velocities and confining pressures, as well as for a system with twice the size of the default model, compared to the estimate (solid line) of per grain KE assuming homogeneous shear between the driving plates. (D) The per grain KE, normalized by $P\Omega_A$ from equation 18 (our estimated RSF a), for the same steady-sliding simulations as in (C), here expressed as a function of the inertial number. The dashed line corresponds to $I_n = 10^{-3}$, which traditionally is considered the limit above which inertial effects become non-negligible. The upward-pointing triangles in (C) and (D) show the "fluctuating granular KE" (δE_k) as defined by Ogawa et al. (1980) and Ogawa (1978) . In the low inertial number regime of interest, the difference between KE and δE_k is insignificant.

where C is the average coordination number (number of contacts per grain), Δ_{ij} is how closely two grain centers approach one another under the contact force F_n, $d()$ in the integral represents an infinitesimal change (not the grain diameter), and the last equality is derived using the nonlinear Hertzian contact law for F_n as a function of grain compression δ_{ij} (equation 8 with no damping, $d_i = d_j$, and $F_n = Pd^2$; d here is grain diameter). If we use D_{mean} for d, and $C \sim 4$ (a value obtained from our simulations), we find $a \sim 0.022$, close to the value determined independently from fitting our velocity-step tests.

There is certainly slop associated with this estimate, including whether the activation volume is more appropriately thought of as a single grain or a few grains that rearrange collectively (as in STZ theory), and whether it is the total normal displacement or the incremental displacement from the background state that determines the activation volume (similar questions pertain to the classical RSF estimate of a, e.g., whether the activation volume corresponds to a single atom or a unit cell). Nonetheless, we find the order-of-magnitude agreement to be encouraging. But this agreement is insufficient; if the granular KE is to play the role of temperature, it must be insensitive to both the sliding speed and the confining pressure, and it is not apparent that this need be the case. Empirically, however, we find that the mean value of granular KE at any particular P changes only modestly over several orders of magnitude variation in V_{lp}, at the low driving speeds of interest (Figure 13C). For comparison, the solid line on the same plot (of slope 2) shows the KE that would result from a layer of uniformly sheared grains as a function of V_{lp}. For $P = 5$ MPa the quasi-constant granular KE intersects this trend at $V_{lp} \sim 2$ m/s, the inertial number $I_n \sim 3 \times 10^{-3}$, and the system is traditionally considered to leave the regime of quasi-static flow (Forterre & Pouliquen, 2008). Furthermore, if we normalize the per grain KE by the estimate of $P\Omega_A$ from equation 18, as in (17), our proposed estimates of a collapse for all confining pressures onto a single curve in the quasi-static regime

(Figure 13D). The prediction is thus that a changes very slowly for a range of shearing velocities and pressures in the quasi-static regime, consistent with both our granular simulations and many laboratory rock and gouge friction experiments.

In Figure 13 we used mean grain kinetic energy as a measure of the effective temperature T_{eff} of the granular gouge. A number of more rigorous thermodynamics- and statistical mechanics-based relationships have been proposed for measuring T_{eff} in granular materials (e.g., the rate of change of energy with entropy); this remains an area of active research (Ono et al., 2002; Blumenfeld & Edwards, 2009; Puckett & Daniels, 2013; Bi et al., 2015). Ono et al. (2002) showed that for zero-temperature foam, seven of these definitions are internally consistent in that they yield the same variation of T_{eff} with shear rate. Further experimental investigations showed that two of these measures of T_{eff} become approximately constant at low shear rates (Song et al., 2005; Corwin et al., 2005). This is similar to our finding in Figure 13E, although these other measures are even more constant than our granular KE at low I_n. Such measurements are necessary to confirm whether different measures of temperature converge toward the same behavior, if they also agree with the variation of kinetic energy, and become nearly constant within the quasi-static regime. Such measurements could elaborate the cause of near constancy of the granular temperature – which to this date remains unknown – by making analogies to the behavior of other glassy materials (like foam) as they approach the glass transition.

6 Conclusions

In this work, we explored the frictional behavior of a granular gouge layer with no time-dependent plasticity at the grain-grain contact scale. We imposed velocity steps over a range of driving velocities and normal stresses that are relevant to earthquake nucleation and laboratory rock friction experiments. We further performed a limited number of slide-hold granular simulations. The system is mechanically stiff enough that, following a step change in driving velocity, the inelastic sliding velocity is essentially constant and variations in the friction coefficient are proportional to variations in log state. We found that the behavior of the granular model appears very similar to the Slip law version of the rate- and state-dependent friction equations, under conditions where the Slip law agrees well with laboratory data, *i.e.* velocity step and slide-hold tests. In particular, we observed that: (i) following velocity steps that vary by several orders of magnitude, friction approaches its future steady-state value over the same sliding distance (or strain, if gouge thickness is varied), (ii) the frictional response of the system to velocity-step increases and decreases is symmetric, (iii) the amplitude of frictional evolution following velocity steps scales with $\log(V_f/V_i)$, and (iv) the ranges of the RSF parameters a (0.020–0.029) and b (0.014–0.023) are not very different from those typically found in laboratory rock and gouge friction experiments. In addition, the slide-hold granular simulations appear to be well described by the Slip law, using parameters derived from fits to the velocity steps, as is the case (or nearly the case) for laboratory friction data. Finally, preliminary slide-hold-slide simulations indicate that the peak stress upon the reslide exceeds the prediction of the Slip law, using the same parameters that fit the hold well, as is also the case with lab data (Bhattacharya et al., 2017).

Future work should include investigating whether the granular model can reproduce observations of the friction peak upon the reslide in slide-hold-slide experiments (often referred to as 'frictional healing') (Marone & Saffer, 2015; Karner & Marone, 1998; Bhattacharya et al., 2017), over a broader range of normal stresses, driving velocities, and system stiffnesses than we have explored thus far; the recent observation that the slip-weakening distance following the reslide increases systematically with log hold time (Bhattacharya et al., 2017); and the friction and thickness changes observed in normal-stress stepping tests (B. Kilgore et al., 2017). These will be important tests for the granular model, as none of the current empirical constitutive relations for the behavior of rock interfaces reproduce these observations acceptably.

The conventional understanding that state evolution in RSF results from contact plasticity suggests that state and gouge thickness are closely related. However, we found that even though gouge thickness seems to be a useful proxy for variations in state following step velocity increases, the gouge thickness evolves over much shorter slip distances than does friction following step decreases. Qualitatively, the asymmetric response of gouge thickness to velocity step increases and decreases appears similar to the asymmetric response of friction (i.e., log state) predicted by the Aging law. Related behavior is seen during load-point holds, where the friction coefficient appears to decay as predicted by the Slip law, implying very little state evolution, while the gouge layer compacts as log time, reminiscent of the (log) state increase predicted by the Aging law. The asymmetric response of the gouge thickness to changes in driving velocity, in conjunction with the symmetric response of the friction coefficient, indicates that gouge thickness is at best an incomplete description of state. The log-time compaction of the gouge during holds in which the friction decay is well described by a law that predicts very little state evolution suggests the same. Aspects of the granular structure other than porosity, such as force fabric and structural anisotropy, must also contribute to in the state of the system (Puckett & Daniels, 2013; Lechenault et al., 2006).

Both the asymmetric response of the gouge thickness to velocity step increases and decreases, and the log-time compaction during load point holds, are predictions of the granular model that seem consistent with laboratory rock and gouge friction experiments. Models of coupled fault gouge dilatancy/pore pressure diffusion (e.g., Segall et al., 2010) are likely to be most consistent with existing lab experiments if porosity is tied to the Aging law for state evolution when state is increasing ($V\theta/D_c < 1$ in equations (2) and (3)), and the Slip law when state is decreasing ($V\theta/D_c > 1$), even while the frictional strength is more accurately modeled by the Slip law under both conditions.

We explored a range of parameters and material properties that could have influenced our observations. We found that grain-grain friction coefficient, restitution coefficient, and grain size had only minor effects on system behavior. Using a system with roughly twice the thickness of the default model, we found that the critical slip distance scales with gouge thickness, and can instead be expressed as a critical strain (of about 13%, when defined as D_c/H). We also examined the influence of changing the grain size distribution from a quasi-normal to a quasi-exponential distribution. This reduced the value of a to about 0.008, near the low end of the range typically cited for rock and gouge. More significantly, we found that changing from a quasi-normal to quasi-exponential grain size distribution changed the steady-state friction from velocity-strengthening to something closer to velocity-neutral. Although within the noise of the simulations the quasi-exponential system could be argued to be strictly velocity-neutral, the close association between the observed velocity-dependence of friction and the clearly non-monotonic steady-state gouge thickness leads us to favor the interpretation that the steady state friction transitions from velocity-weakening to velocity-strengthening with increasing slip speed. A non-monotonic dependence of steady-state friction on driving velocity has not often been observed in numerical simulations of frictional granular systems (da Cruz et al., 2005; Kamrin & Koval, 2014; Koval et al., 2009; MiDi, 2004), but within our adopted range of dimensionless pressures and inertial numbers it is consistent with recent theoretical predictions (DeGiuli & Wyart, 2017). The effect of grain size distribution was not explored by DeGiuli and Wyart (2017), however. In the velocity-strengthening regime, where the quasi-exponential gouge layer dilates with increasing slip speed, following a velocity step the layer approaches its new steady-state thickness monotonically, just as does the velocity-strengthening gouge with the quasi-normal size distribution. In the velocity-weakening regime, however, the gouge thickness for the quasi-exponential system varies non-monotonically following a velocity step, for example first compacting following a step decrease before dilating by a larger amount with continued slip. This initial response seems consistent with a positive direct velocity effect, and is consistent with the observed compaction during holds for the quasi-exponential system, but the non-monotonic evolution of thickness with slip is yet another indication that there is not a simple relation between gouge porosity and state, and we do not understand its cause.

By making an analogy between granular rearrangements in a potential energy landscape and a thermally-activated Arrhenius process, we estimated the magnitude of direct velocity effect (the RSF parameter a) in our model. For this purpose, we used the mean kinetic energy of grains as a measure of granular temperature, and assumed that this was equivalent to the thermodynamic temperature in a thermally-activated process. We found a value of a close to that obtained independently from fitting our velocity-step tests. Furthermore, this value was found to be independent of confining stress and nearly independent of slip speed. This nearly constant value of a is consistent with our simulation results and with much lab data.

The successful adoption here of the granular temperature may motivate its future implementation as a state variable for granular rate- and state-dependent friction. In standard thermodynamics, involving thermal materials, energy is the conserved property. However, the granular materials in our simulations, and in many others in the physics literature, are athermal, in the sense that the actual temperature plays no role. Recent progress in the granular physics community points toward a revised version of granular temperature, called keramicity and defined in the stress ensemble, where instead of energy the conserved quantity is the force-moment tensor of the granular packing (Bi et al., 2015). Ideally, one would like to devise a state variable that would obey the laws of thermodynamics for granular systems and be path- and protocol-independent. It would be interesting to investigate whether a state variable defined in the stress ensemble could be used for effectively describing the rate- and state-dependent frictional behavior of rocks.

While our observations here focused on rock gouge and the frictional behavior of fault rocks, they could be potentially relevant for transient frictional behavior and hysteresis of a broad range of disordered Earth materials, such as soils on hillslopes (Ferdowsi et al., 2018; Handwerger et al., 2016), fluvial sediments (Houssais et al., 2015; J. P. Johnson, 2016; Masteller et al., 2019), and sub-glacial till (Rathbun et al., 2008).

Appendix A Dimensionless parameters

The adopted DEM model has many dimensionless parameters, each of which could potentially affect the system behavior. However, only a few of these seem to be significant. Here we give a full accounting of these parameters, along with a qualitative assessment of their relevance to the observed RSF parameters in the slow shearing regime of interest.

Table A1. DEM parameters for steady-sliding simulations.

Symbol	Parameter	Units
D	Median grain diameter	[m]
H	Nominal gouge thickness	[m]
L_x	Domain length in slip direction	[m]
L_y	Domain length in slip-perpendicular direction	[m]
k_n	Grain normal contact stiffness	[Pa]
k_t	Grain shear contact stiffness	[Pa]
ϵ_n	Grain normal restitution coefficient	[ ]
ϵ_t	Grain shear restitution coefficient	[ ]
μ_g	Grain-grain friction coefficient	[ ]
ρ	Grain density	[kg m^{-3}]
V_{lp}	Driving velocity	[m s^{-1}]
σ_n (P)	Applied normal stress	[Pa]
k_{sp}	Driving spring stiffness	[Pa m^{-1}]
g	Gravitational acceleration	[m s^{-2}]
Δt	Numerical time step	[s]

Neglecting parameters associated with the adopted grain size distribution, Table A1 lists 15 independent dimensional parameters using 3 dimensions (writing Pa as kg m^{-1} s^{-2}), implying that 12 dimensionless parameters govern the system. Some of the parameters in Table A1 can be considered as equivalent to an equal number of different parameters; for example, the grain normal and shear contact stiffnesses are derived from the elastic shear and Young's moduli (G and E), and the normal and shear restitution coefficients are derived from the normal and shear damping coefficients γ_n and

γ_t. Additional parameters depend upon those listed; for example, the grain mass m and the bulk density ρ_H and shear modulus G_H, as well as the measured friction coefficient.

Before listing dimensionless parameters, we introduce some relevant time scales:

1. t_γ, time scale for bulk strain of 1: H/V_{lp}.
2. t_w, time scale for elastic shear wave propagation across layer: $H/\sqrt{G_H/\rho_H}$.
3. t_i, inertial time scale for an initially stationary a grain to move a distance D, given an applied force PD^2: $D\sqrt{\rho/P}$
4. t_{col}, collision time (obtained by solving equation (12) in the text).

Table A2 lists a reasonable set of choices for the 12 dimensionless parameters. Three involve ratios of lengths. It has been proposed that the ratio H/D determines the ability of the gouge to localize deformation, with no localization for values $\lesssim 10$ (Tsai & Gollub, 2005). We see no localization in the velocity profiles for our default model with $H/D \sim 13.3$, or in the model with $H/D = 24$ and L_x/H and L_y/H unchanged. We also see no change in the RSF parameters between the two simulations, provided we speak of a critical strain rather than a critical slip distance D_c (Figure 6). The ratios L_x/H and L_y/H are not expected to be significant as long as they are sufficiently large; if force chains typically form at $\sim 45°$ then L_x/H should at a minimum exceed 1. We see no significant difference between $L_x/H = 1.5$ and $L_x/H = 5$ for both normal and exponential grain size distributions, other than the expected result that simulations with $L_x/H = 5$ exhibit less variability during steady sliding.

Table A2. DEM governing parameters.

H/D; L_x/H; L_y/H
ϵ_n; ϵ_t; μ_g
k_n/k_t; $k_{sp}/(G/H)$; $\rho gH/P$
$\Delta t/t_c$
t_i/t_γ (Inertial number I_n, equal to $(V_{lp}/H)D\sqrt{\rho/P}$
$(P/E)^{2/3}$ (dimensionless pressure)

We have varied ϵ_n over nearly the full range of 0 to 1. Consistent with previous results for steady-state friction (MiDi, 2004), we find negligible influence of the restitution coefficients on the RSF parameters in the low-I_n regime of interest (Supplementary Figure S3). We have always assumed that the damping coefficients satisfy $\gamma_t = 0.5\gamma_n$, the default for LAMMPS, from which the restitution coefficients are derived, but given the existing results we expect no significant change for $\gamma_t \neq 0.5\gamma_n$. We also see no significant changes in the RSF parameters when doubling μ_g from the default value of 0.5 to 1.0 (Supplementary Figure S6). This is consistent with previous studies that show little influence of μ_g on steady-state friction (MiDi, 2004).

The ratio k_n/k_t is fixed by the elastic moduli of the grains and is not a free parameter. The ratio $k_{sp}/(G/H)$ controls the elastic deformation of the driving spring to that of the gouge layer (the more relevant bulk gouge shear modulus G_H depends upon G and the granular packing). We made k_{sp} extremely large, to make the effective stiffness of the system as large as possible; this ensures that sliding velocity following a step change in V_{lp} is constant, such that changes in friction correspond directly to changes in log(state), facilitating a "by eye" comparison of the measured friction transient to different state evolution laws. Significantly reducing $k_{sp}/(G/H)$ will change the loading history of the gouge layer for a given V_{lp} history, but traditionally the RSF parameters are assumed to be independent of loading history. The ratio $\rho gH/P$ determines the relative magnitude of the gravitational stress at the base of the gouge layer to the applied stress; in our simulations it is so low (10^{-6} to 10^{-8}) that we expect it to be negligible, although it may lead to some grain sorting during the packing of the gouge layer prior to imposing the confining pressure. In the future it would make sense to dispense with gravity during the sliding and most of the packing phases.

For numerical accuracy we employ $\Delta t/t_{col} = 0.01$, small enough that it does not influence the simulations.

The inertial number I_n, equal to t_i/t_γ, is a well-established control parameter for granular systems, but from the figures in this paper it does not affect the RSF parameters much. This is consistent with many laboratory rock and gouge friction experiments.

The dimensionless pressure $(P/E)^{2/3}$ is equal to the grain strain (grain compression at a contact divided by the initial grain radius) under the Hertzian contact law. For P from 1 to 50 MPa, this ratio varies from 0.7×10^{-3} to 10^{-2}, near to but perhaps not within the "rigid grain" limit (DeGiuli & Wyart, 2017). We find that the RSF parameters vary only modestly, and not necessarily consistently, over this interval (Table 5.2.1).

This information can be used to extrapolate beyond the simulations already run. For example, we use a relatively large D_{mean} of 3 mm, but from Table A2, if we reduce the grain size and all model dimensions by the same factor (say 2 orders of magnitude) and keep V_{lp} and all other parameters the same, we change nothing other than to increase $k_{sp}/(G_H/H)$ and decrease $\rho g H/P$ by the same 2 orders of magnitude. These ratios were already so large and so small that we expect to see no significant changes to the model output, consistent with Figure 9.

In summary, despite the large number of dimensionless parameters in Table A2, remarkably few of these are free parameters available for tuning the values of the RSF coefficients. Their influence might be largest on the value of $(a-b)$, as this depends upon the difference between two numbers of comparable magnitude. Significantly, the sign of $(a-b)$ seems sensitive to the grain size distribution. This is a parameter that, along with grain shape and perhaps others, is not referenced in Table A1.

Appendix B The inertial contribution to the measured shear stress

Equation (13) in the main text assumes that the elastic component of the gouge deformation occurs quasi-statically and uniformly across the gouge, such that for constant load-point and sliding velocities the shear stress increases linearly with time and load-point displacement. However, for a linearly elastic system, following a sudden change of upper plate velocity ΔV_{pl}, a shear wave traverses the layer that, until the arrival of the reflected wave from the stationary lower plate, imposes an instantaneous shear stress change at the base of the upper plate given by

$$\Delta\tau_{\text{inertial}} = G_H \frac{\Delta V_{pl}}{\beta} = \Delta V_{pl}\sqrt{G_H \rho_H}\,, \tag{B1}$$

where $\beta = \sqrt{G_H/\rho_H}$ is the elastic shear wave speed, with G_H being the shear modulus and ρ_H the density of the gouge layer (Rice, 1993). Dividing this by the normal stress gives an estimate of the inertial contribution to the "apparent" direct velocity effect,

$$\Delta\mu_{\text{inertial}} = \Delta V_{pl}\sqrt{G_H \rho_H}/\sigma_n\,. \tag{B2}$$

For the example of the 4-order velocity increase to $V_f = 2$ m/s in Figure 3A, we see an instantaneous, not linear-with-time, apparent $\Delta\mu_{\text{inertial}}$ of about 0.19. Plugging this value into the left side of (B2), and on the right 5 MPa for σ_n and a typical porosity of 0.45 to estimate ρ_H, we calculate $G_H = 165$ MPa. This is just over half the 270-310 MPa we estimated from the reloading (at much lower slip speeds) of the gouge following long holds (Figure B1), but it is certainly possible that at the large stresses associated with the 4-order velocity jump, some inelastic deformation is occurring.

Note that Figure 9B shows a snapshot in which the shear wave front following a 1-order velocity jump (to 0.1 m/s) has yet to traverse the gouge layer. The post-jump displacement of the upper plate is $10^{-3}D_{mean}$, or 3×10^{-6} m, in (at V_{lp} = 0.1 m/s) 3×10^{-5} s, and the shear wave has progressed approximately 0.02 m, implying a propagation velocity of ~670 m/s. Setting this equal to $\sqrt{G_H/\rho_H}$ and estimating ρ_H as above, we can derive a third independent estimate of G_H: 610 MPa, about twice the estimate from Figure B1. As we have not investigated in detail the nature of the shear wave propagation across the gouge layer, we continue to use our mid-range estimate of $G_H \sim 300$ MPa, consistent with our nearly quasi-static reloading simulations ($V_{lp} = 2\times10^{-2}$ m/s), with previous experimental, numerical, and theoretical estimates for granular systems under comparable conditions (Yin, 1993; Domenico, 1977; Makse et al., 1999), and with standard methods of estimating G in laboratory rock and gouge friction experiments (e.g., Bhattacharya et al., 2017). As we note in the main text, 300 MPa is large enough that variations in G_H of a factor of 2 do not change the Slip law fits to our simulated velocity steps, and do not change the slope of the slip law prediction at large hold times in Figure 12.

It is clear that for any value of G_H in the vicinity of 300 MPa, for $V_f = 2$ m/s inertia contributes significantly to the apparent $\Delta\mu$ for early times. However, note that once the steady-state velocity profile in the gouge is reached, the contribution from bulk inertia to the measured $\Delta\mu$ at later times is zero. The approach to that steady-state velocity profile is likely a complex process involving multiple reflections from the bounding rigid plates. We can make an estimate of $\Delta\mu_{\text{inertial}}$ in this case from the inertial force per area A required to change the velocity profile from one steady state to another over a time Δt:

$$\Delta\mu_{\text{inertial}} = \frac{m\ddot{x}}{\sigma_n A} = \frac{\rho_H H}{\sigma_n}\frac{\Delta V_{pl}/2}{\Delta t}\,, \tag{B3}$$

where $\ddot{x}$ is the spatially-averaged acceleration of the gouge particles and $\Delta V_{pl}/2$ comes from assuming the steady-state velocity profile to vary linearly across the gouge layer. Note that $\Delta\mu_{\text{inertial}}$ is proportional to $1/\Delta t$ as well as to ΔV_{pl}. For example, peak friction for $V_f = 2$ m/s in Figure 3 is reached at 6×10^{-4} s. If this is the time at which the steady-state velocity profile is reached (roughly 5 times the 2-way shear wave travel time across the gouge as estimated from Figure 9B), the inertial contribution to the apparent $\Delta\mu$ would average only 0.018 up to that point (11% of the plotted peak value), would likely be lower at that slip distance, and would be zero at greater distances. If the steady-state velocity profile was not reached until a slip distance of D_{mean}, the contribution to the measured friction up to that point would average more than a factor of two smaller. In light of these results, we conclude that inertia can contribute modestly (or zero) to the measured friction in the vicinity of the friction peak for $V_f = 2$ m/s in Figure 3, but that it provides a negligible contribution to the overall Slip law fit to that friction curve.

For the 10-times-smaller jump to $V_f = 0.2$ m/s, the inertial contribution to the measured friction would be 10 times smaller from equation (B2), as well as from (B3) assuming that the same time Δt is required to reach the new steady-state velocity profile. For this velocity step the peak friction does not occur until a slip distance of $\sim 0.4D_{mean}$, at which point the steady-state velocity profile is almost certainly established (see Figures 9C and D for velocity profiles at slip distances 40 and 4 times smaller, for $V_f = 0.1$ m/s), and the contribution from bulk inertia would be zero (if not, from (B3) the average contribution up to that point would be 0.0019, which at the scale of Figure 3A is completely negligible). We conclude that bulk inertia plays no discernible role in our simulated velocity steps where the larger (initial or final) slip speed is 0.2 m/s or smaller, and that even at 2 m/s inertia will only affect the friction curves significantly for slip distances smaller than some tenths of D_{mean}.

Acknowledgments

BF acknowledges support from the Department of Geosciences, Princeton University, in form of a Harry H. Hess postdoctoral fellowship, and from NSF award EAR-1547286 and the US Geological Survey (USGS), Department of the Interior, award G19AP00048, both to AMR. BF performed some slide-hold-slide tests during his PhD research with the granular physics model he developed in his PhD. Some elements of the current model, which is distinct from the model in his PhD,

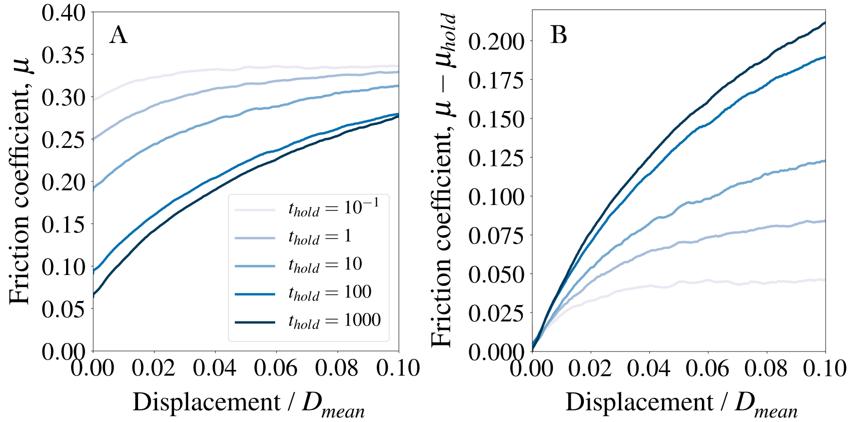

Figure B1. (A) The variation of friction coefficient with load-point displacement for the reslide portion of several slide-hold-reslide simulations (obtained from the default model with $V_{lp} = 2 \times 10^{-2}$ m/s and $\sigma_n = 5$ MPa). In (B), the friction coefficient at the end of the hold is subtracted from the signals, so the initial slopes of the reslide curves can be more easily compared. From the asymptotic slope at zero displacement (using the longest hold over a load-point displacement of $0.008 D_{mean}$) we estimate an elastic shear modulus of $\sim 270 - 310$ MPa.

were developed during BF's stay at the University of Pennsylvania, partially supported by the 2016 Southern California Earthquake Center (SCEC) award 16059 to David L. Goldsby. A study on the granular origins of rate- and state-dependent friction for fault gouge was also proposed in that same award to David L. Goldsby. BF benefited from conversations with Chris Marone, Pathikrit Bhattacharya, Anders Damsgaard, Nicholas M. Beeler, Heather Savage, Emily Brodsky, Andrea J. Liu, Corey O'Hern, Troy Shinbrot, Norman Sleep, Rob Skarbek, Paul Segall, Karen E. Daniels, Shmuel Rubinstein, Rob Viesca, Melodie French, Julia Morgan, Jean M. Carlson, Ahmed Elbanna, Andreas Kronenberg, David Sparks, and Hiroko Kitajima. AR benefited from a subset of those. BF would also like to acknowledge support he has received from D. J. Jerolmack and D. L. Goldsby, and the insightful discussions he had with D. J. Jerolmack, D. L. Goldsby, C. A. Thom, and Carlos P. Ortiz on this topic during 2015-2016. Parallel programs were run on computers provided by the Princeton Institute for Computational Science and Engineering (PICSciE). The 3-D visualizations of the model were performed using the open-source visualization software "The Persistence of Vision Raytracer" POV-Ray (http://www.povray.org). Most of the data analysis were carried out using the open-source Python library, NumPy (https://numpy.org). The 2-D plots were made with the Python library Matplotlib (www.matplotlib.org). The computer codes for LAMMPS simulations of this paper with the information about the version of LAMMPS used for the simulations, are available on the Dryad digital repository at *https://doi.org/10.5061/dryad.2z34tmphk*. We thank two anonymous reviewers whose suggestions helped to improve and clarify this paper. The views and conclusions contained in this document are those of the authors and should not be interpreted as necessarily representing the official policies, either expressed or implied, of the U.S. Government.

References

Abe, S., Dieterich, J. H., Mora, P., & Place, D. (2002). Simulation of the influence of rate-and state-dependent friction on the macroscopic behavior of complex fault zones with the lattice solid model. *pure and applied geophysics*, *159*(9), 1967–1983.

Abe, S., & Mair, K. (2009). Effects of gouge fragment shape on fault friction: New 3d modelling results. *Geophysical Research Letters*, *36*(23).

Aghababaei, R., Brink, T., & Molinari, J.-F. (2018). Asperity-level origins of transition from mild to severe wear. *Physical review letters*, *120*(18), 186105.

Aharonov, E., & Sparks, D. (2002). Shear profiles and localization in simulations of granular materials. *Physical Review E*, *65*(5), 051302.

Aharonov, E., & Sparks, D. (2004). Stick-slip motion in simulated granular layers. *Journal of Geophysical Research: Solid Earth*, *109*(B9).

Amon, A., Bruand, A., Crassous, J., Clément, E., et al. (2012). Hot spots in an athermal system. *Physical review letters*, *108*(13), 135502.

Ampuero, J.-P., & Rubin, A. M. (2008). Earthquake nucleation on rate and state faults–aging and slip laws. *Journal of Geophysical Research: Solid Earth*, *113*(B1).

An, L.-J., & Sammis, C. G. (1994). Particle size distribution of cataclastic fault materials from southern california: A 3-d study. *Pure and Applied Geophysics*, *143*(1-3), 203–227.

Anthony, J. L., & Marone, C. (2005). Influence of particle characteristics on granular friction. *Journal of Geophysical Research: Solid Earth*, *110*(B8).

Baumberger, T., Berthoud, P., & Caroli, C. (1999). Physical analysis of the state-and rate-dependent friction law. ii. dynamic friction. *Physical Review B*, *60*(6), 3928.

Baumberger, T., & Caroli, C. (2006). Solid friction from stick–slip down to pinning and aging. *Advances in Physics*, *55*(3-4), 279–348.

Beeler, N., & Tullis, T. (1997). The roles of time and displacement in velocity-dependent volumetric strain of fault zones. *Journal of Geophysical Research: Solid Earth*, *102*(B10), 22595–22609.

Beeler, N., Tullis, T., Blanpied, M., & Weeks, J. (1996). Frictional behavior of large displacement experimental faults. *Journal of Geophysical Research: Solid Earth*, *101*(B4), 8697–8715.

Beeler, N., Tullis, T., & Weeks, J. (1994). The roles of time and displacement in the evolution effect in rock friction. *Geophysical Research Letters*, *21*(18), 1987–1990.

Behringer, R. P., Bi, D., Chakraborty, B., Henkes, S., & Hartley, R. R. (2008). Why do granular materials stiffen with shear rate? test of novel stress-based statistics. *Physical review letters*, *101*(26), 268301.

Berthoud, P., Baumberger, T., G'sell, C., & Hiver, J.-M. (1999). Physical analysis of the state-and rate-dependent friction law: Static friction. *Physical review B*, *59*(22), 14313.

Bhattacharya, P., Rubin, A. M., Bayart, E., Savage, H. M., & Marone, C. (2015). Critical evaluation of state evolution laws in rate and state friction: Fitting large velocity steps in simulated fault gouge with time-, slip-, and stress-dependent constitutive laws. *Journal of Geophysical Research: Solid Earth*, *120*(9), 6365–6385.

Bhattacharya, P., Rubin, A. M., & Beeler, N. M. (2017). Does fault strengthening in laboratory rock friction experiments really depend primarily upon time and not slip? *Journal of Geophysical Research: Solid Earth*.

Bi, D., Henkes, S., Daniels, K. E., & Chakraborty, B. (2015). The statistical physics of athermal materials. *Annu. Rev. Condens. Matter Phys.*, *6*(1), 63–83.

Bililign, E. S., Kollmer, J. E., & Daniels, K. E. (2019). Protocol dependence and state variables in the force-moment ensemble. *Physical review letters*, *122*(3), 038001.

Billi, A. (2005). Grain size distribution and thickness of breccia and gouge zones from thin (¡ 1 m) strike-slip fault cores in limestone. *Journal of Structural Geology*, *27*(10), 1823–1837.

Blanpied, M., Marone, C., Lockner, D., Byerlee, J., & King, D. (1998). Quantitative measure of the variation in fault rheology due to fluid-rock interactions. *Journal of Geophysical Research: Solid Earth*, *103*(B5), 9691–9712.

Blumenfeld, R., & Edwards, S. F. (2009). On granular stress statistics: Compactivity, angoricity, and some open issues. *The Journal of Physical Chemistry B*, *113*(12), 3981–3987.

Bouzid, M., Izzet, A., Trulsson, M., Clément, E., Claudin, P., & Andreotti, B. (2015). Non-local rheology in dense granular flows. *The European Physical Journal E*, *38*(11), 125.

Brilliantov, N. V., Spahn, F., Hertzsch, J.-M., & Pöschel, T. (1996). Model for collisions in granular gases. *Physical review E*, *53*(5), 5382.

Chester, F. M. (1994). Effects of temperature on friction: Constitutive equations and experiments with quartz gouge. *Journal of Geophysical Research: Solid Earth*, *99*(B4), 7247–7261.

Corwin, E. I., Jaeger, H. M., & Nagel, S. R. (2005). Structural signature of jamming in granular media. *Nature*, *435*(7045), 1075.

da Cruz, F., Emam, S., Prochnow, M., Roux, J.-N., & Chevoir, F. (2005). Rheophysics of dense granular materials: Discrete simulation of plane shear flows. *Physical Review E*, *72*(2), 021309.

Darnige, T., Bruand, A., Clement, E., et al. (2011). Creep and fluidity of a real granular packing near jamming. *Physical review letters*, *107*(13), 138303.

Daub, E. G., & Carlson, J. M. (2008). A constitutive model for fault gouge deformation in dynamic rupture simulations. *Journal of Geophysical Research: Solid Earth*, *113*(B12).

de Coulomb, A. F., Bouzid, M., Claudin, P., Clément, E., & Andreotti, B. (2017). Rheology of granular flows across the transition from soft to rigid particles. *Physical Review Fluids*, *2*(10), 102301.

DeGiuli, E., & Wyart, M. (2017). Friction law and hysteresis in granular materials. *Proceedings of the National Academy of Sciences*, *114*(35), 9284–9289.

Dieterich, J. (1994). A constitutive law for rate of earthquake production and its application to earthquake clustering. *Journal of Geophysical Research: Solid Earth*, *99*(B2), 2601–2618.

Dieterich, J. H. (1972). Time-dependent friction in rocks. *Journal of Geophysical Research*, *77*(20), 3690–3697.

Dieterich, J. H. (1978). Time-dependent friction and the mechanics of stick-slip. In *Rock friction and earthquake prediction* (pp. 790–806). Springer.

Dieterich, J. H. (1979). Modeling of rock friction: 1. experimental results and constitutive equations. *Journal of Geophysical Research: Solid Earth*, *84*(B5), 2161–2168.

Dieterich, J. H. (1992). Earthquake nucleation on faults with rate-and state-dependent strength. *Tectonophysics*, *211*(1-4), 115–134.

Dieterich, J. H., & Kilgore, B. (1996). Implications of fault constitutive properties for earthquake prediction. *Proceedings of the National Academy of Sciences*, *93*(9), 3787–3794.

Dieterich, J. H., & Kilgore, B. D. (1994). Direct observation of frictional contacts: New insights for state-dependent properties. *Pure and Applied Geophysics*, *143*(1-3), 283–302.

Dieterich, J. H., et al. (1981). Constitutive properties of faults with simulated gouge. *Mechanical Behavior of*.

Dijksman, J. A., Wortel, G. H., van Dellen, L. T., Dauchot, O., & van Hecke, M. (2011). Jamming, yielding, and rheology of weakly vibrated granular media. *Physical review letters*, *107*(10), 108303.

Domenico, S. (1977). Elastic properties of unconsolidated porous sand reservoirs. *Geophysics*, *42*(7), 1339–1368.

Ferdowsi, B., Griffa, M., Guyer, R., Johnson, P., Marone, C., & Carmeliet, J. (2013). Microslips as precursors of large slip events in the stick-slip dynamics of sheared granular layers: A discrete element model analysis. *Geophysical Research Letters*, *40*(16), 4194–4198.

Ferdowsi, B., Ortiz, C. P., & Jerolmack, D. J. (2018). Glassy dynamics of landscape evolution. *Proceedings of the National Academy of Sciences*, *115*(19), 4827–4832.

Forterre, Y., & Pouliquen, O. (2008). Flows of dense granular media. *Annu. Rev. Fluid Mech.*, *40*, 1–24.

Frye, K. M., & Marone, C. (2002). Effect of humidity on granular friction at room temperature. *Journal of Geophysical Research: Solid Earth*, *107*(B11), ETG–11.

Handwerger, A. L., Rempel, A. W., Skarbek, R. M., Roering, J. J., & Hilley, G. E. (2016). Rate-weakening friction characterizes both slow sliding and catastrophic failure of landslides. *Proceedings of the National Academy of Sciences*, *113*(37), 10281–10286.

Hartley, R., & Behringer, R. (2003). Logarithmic rate dependence of force networks in sheared granular materials. *Nature*, *421*(6926), 928.

Hatano, T. (2007). Power-law friction in closely packed granular materials. *Physical Review E*, *75*(6), 060301.

Hatano, T. (2009). Scaling of the critical slip distance in granular layers. *Geophysical Research Letters*, *36*(18).

Hatano, T. (2015). Friction laws from dimensional-analysis point of view. *Geophysical Journal International*, *202*(3), 2159–2162.

Hazzard, J. F., & Mair, K. (2003). The importance of the third dimension in granular shear. *Geophysical Research Letters*, *30*(13).

Heslot, F., Baumberger, T., Perrin, B., Caroli, B., & Caroli, C. (1994). Creep, stick-slip, and dry-friction dynamics: Experiments and a heuristic model. *Physical review E*, *49*(6), 4973.

Houssais, M., Ortiz, C. P., Durian, D. J., & Jerolmack, D. J. (2015). Onset of sediment transport is a continuous transition driven by fluid shear and granular creep. *Nature communications*, *6*.

Johnson, J. P. (2016). Gravel threshold of motion: a state function of sediment transport disequilibrium? *Earth Surface Dynamics*, *4*(3), 685–703.

Johnson, K. L. (1987). *Contact mechanics*. Cambridge University Press.

Kamrin, K., & Koval, G. (2014). Effect of particle surface friction on nonlocal constitutive behavior of flowing granular media. *Computational Particle Mechanics*, *1*(2), 169–176.

Karner, S. L., & Marone, C. (1998). The effect of shear load on frictional healing in simulated fault gouge. *Geophysical research letters*, *25*(24), 4561–4564.

Kato, N., & Tullis, T. E. (2001). A composite rate-and state-dependent law for rock friction. *Geophysical research letters*, *28*(6), 1103–1106.

Kilgore, B., Beeler, N. M., Lozos, J., & Oglesby, D. (2017). Rock friction under variable normal stress. *Journal of Geophysical Research: Solid Earth*, *122*(9), 7042–7075.

Kilgore, B. D., Blanpied, M. L., & Dieterich, J. H. (1993). Velocity dependent friction of granite over a wide range of conditions. *Geophysical Research Letters*, *20*(10), 903–906.

Koval, G., Roux, J.-N., Corfdir, A., & Chevoir, F. (2009). Annular shear of cohesionless granular materials: From the inertial to quasistatic regime. *Physical Review E*, *79*(2), 021306.

Kuwano, O., Ando, R., & Hatano, T. (2013). Crossover from negative to positive shear rate dependence in granular friction. *Geophysical research letters*, *40*(7), 1295–1299.

Landau, L. D., & Lifshitz, E. M. (1959). Theory of elasticity.

Lapusta, N., Rice, J. R., Ben-Zion, Y., & Zheng, G. (2000). Elastodynamic analysis for slow tectonic loading with spontaneous rupture episodes on faults with rate-and state-dependent friction. *Journal of Geophysical Research: Solid Earth*, *105*(B10), 23765–23789.

Le Bouil, A., Amon, A., McNamara, S., & Crassous, J. (2014). Emergence of cooperativity in plasticity of soft glassy materials. *Physical review letters*, *112*(24), 246001.

Lechenault, F., da Cruz, F., Dauchot, O., & Bertin, E. (2006). Free volume distributions and compactivity measurement in a bidimensional granular packing. *Journal of Statistical Mechanics: Theory and Experiment*, *2006*(07), P07009.

Lemaître, A. (2002). Rearrangements and dilatancy for sheared dense materials. *Physical Review Letters*, *89*(19), 195503.

Li, Q., Tullis, T. E., Goldsby, D., & Carpick, R. W. (2011). Frictional ageing from interfacial bonding and the origins of rate and state friction. *Nature*, *480*(7376), 233.

Li, T., & Rubin, A. M. (2017). A microscopic model of rate and state friction evolution. *Journal of Geophysical Research: Solid Earth*, *122*(8), 6431–6453.

Lieou, C. K., Daub, E. G., Guyer, R. A., Ecke, R. E., Marone, C., & Johnson, P. A. (2017). Simulating stick-slip failure in a sheared granular layer using a physics-based constitutive model. *Journal of Geophysical Research: Solid Earth*, *122*(1), 295–307.

Ma, X., & Elbanna, A. (2018). Strain localization in dry sheared granular materials: A compactivity-based approach. *Physical Review E*, *98*(2), 022906.

Mair, K., Frye, K. M., & Marone, C. (2002). Influence of grain characteristics on the friction of granular shear zones. *Journal of Geophysical Research: Solid Earth*, *107*(B10), ECV–4.

Mair, K., & Marone, C. (1999). Friction of simulated fault gouge for a wide range of velocities and normal stresses. *Journal of Geophysical Research: Solid Earth*, *104*(B12), 28899–28914.

Makse, H. A., Gland, N., Johnson, D. L., & Schwartz, L. (2004). Granular packings: Nonlinear elasticity, sound propagation, and collective relaxation dynamics. *Physical Review E*, *70*(6), 061302.

Makse, H. A., Gland, N., Johnson, D. L., & Schwartz, L. M. (1999). Why effective medium theory fails in granular materials. *Physical Review Letters*, *83*(24), 5070.

Manning, M. L., Langer, J. S., & Carlson, J. (2007). Strain localization in a shear transformation zone model for amorphous solids. *Physical review E*, *76*(5), 056106.

Marone, C. (1998a). The effect of loading rate on static friction and the rate of fault healing during the earthquake cycle. *Nature*, *391*(6662), 69.

Marone, C. (1998b). Laboratory-derived friction laws and their application to seismic faulting. *Annual Review of Earth and Planetary Sciences*, *26*(1), 643–696.

Marone, C., & Kilgore, B. (1993). Scaling of the critical slip distance for seismic faulting with shear strain in fault zones. *Nature*, *362*(6421), 618.

Marone, C., Raleigh, C. B., & Scholz, C. (1990). Frictional behavior and constitutive modeling of simulated fault gouge. *Journal of Geophysical Research: Solid Earth*, *95*(B5), 7007–7025.

Marone, C., & Saffer, D. (2015). The mechanics of frictional healing and slip instability during the seismic cycle. In G. Schubert (Ed.), *Treatise on geophysics (second edition)* (Second Edition ed., p. 111 - 138). Oxford: Elsevier. Retrieved from `http://www.sciencedirect.com/science/article/pii/B9780444538024000920` doi: https://doi.org/10.1016/B978-0-444-53802-4.00092-0

Marone, C., & Scholz, C. (1989). Particle-size distribution and microstructures within simulated fault gouge. *Journal of Structural Geology*, *11*(7), 799–814.

Masteller, C. C., Finnegan, N. J., Turowski, J. M., Yager, E. M., & Rickenmann, D. (2019). History-dependent threshold for motion revealed by continuous bedload transport measurements in a steep mountain stream. *Geophysical Research Letters*, *46*(5), 2583–2591.

MiDi, G. (2004). On dense granular flows. *European Physical Journal E–Soft Matter*, *14*(4).

Mindlin, R. D. (1949). Compliance of elastic bodies in contact. *J. Appl. Mech., ASME*, *16*, 259–268.

Morgan, J. K. (2004). Particle dynamics simulations of rate-and state-dependent frictional sliding of granular fault gouge. In *Computational earthquake science part i* (pp. 1877–1891). Springer.

Morrow, C. A., & Byerlee, J. D. (1989). Experimental studies of compaction and dilatancy during frictional sliding on faults containing gouge. *Journal of Structural Geology*, *11*(7), 815–825.

Murphy, K. A., Dahmen, K. A., & Jaeger, H. M. (2019, Jan). Transforming mesoscale granular plasticity through particle shape. *Phys. Rev. X*, *9*, 011014. Retrieved from `https://link.aps.org/doi/10.1103/PhysRevX.9.011014` doi: 10.1103/PhysRevX.9.011014

Murphy, K. A., MacKeith, A. K., Roth, L. K., & Jaeger, H. M. (2019). The intertwined roles of particle shape and surface roughness in controlling the shear strength of a granular material. *arXiv preprint arXiv:1902.03280*.

Nakatani, M. (2001). Conceptual and physical clarification of rate and state friction: Frictional sliding as a thermally activated rheology. *Journal of Geophysical Research: Solid Earth*, *106*(B7), 13347–13380.

Ogawa, S. (1978). Multitemperature theory of granular materials. In *Proc. of the us-japan seminar on continuum mechanical and statistical approaches in the mechanics of granular materials, 1978* (pp. 208–217).

Ogawa, S., Umemura, A., & Oshima, N. (1980). On the equations of fully fluidized granular materials. *Zeitschrift für angewandte Mathematik und Physik ZAMP*, *31*(4), 483–493.

Ono, I. K., O'Hern, C. S., Durian, D. J., Langer, S. A., Liu, A. J., & Nagel, S. R. (2002). Effective temperatures of a driven system near jamming. *Physical review letters*, *89*(9), 095703.

Perrin, H., Clavaud, C., Wyart, M., Metzger, B., & Forterre, Y. (2019). Interparticle friction leads to non-monotonic flow curves and hysteresis in viscous suspensions. *arXiv preprint arXiv:1904.03918*.

Puckett, J. G., & Daniels, K. E. (2013). Equilibrating temperaturelike variables in jammed granular subsystems. *Physical Review Letters*, *110*(5), 058001.

Rathbun, A. P., & Marone, C. (2013). Symmetry and the critical slip distance in rate and state friction laws. *Journal of Geophysical Research: Solid Earth*, *118*(7), 3728–3741.

Rathbun, A. P., Marone, C., Alley, R. B., & Anandakrishnan, S. (2008). Laboratory study of the frictional rheology of sheared till. *Journal of Geophysical Research: Earth Surface*, *113*(F2).

Rice, J. R. (1993). Spatio-temporal complexity of slip on a fault. *Journal of Geophysical Research: Solid Earth*, *98*(B6), 9885–9907.

Rice, J. R. (2006). Heating and weakening of faults during earthquake slip. *Journal of Geophysical Research: Solid Earth*, *111*(B5).

Rice, J. R., Lapusta, N., & Ranjith, K. (2001). Rate and state dependent friction and the stability of sliding between elastically deformable solids. *Journal of the Mechanics and Physics of Solids*, *49*(9), 1865–1898.

Ruina, A. (1983). Slip instability and state variable friction laws. *Journal of Geophysical Research: Solid Earth (1978–2012)*, *88*(B12), 10359–10370.

Ruina, A. L. (1980). Friction laws and instabilities: a quasi-static analysis of some dry friction behaviour. *Ph. D. thesis, Division of Engineering, Brown University*.

Salerno, K. M., Bolintineanu, D. S., Grest, G. S., Lechman, J. B., Plimpton, S. J., Srivastava, I., & Silbert, L. E. (2018). Effect of shape and friction on the packing and flow of granular materials. *Physical Review E*, *98*(5), 050901.

Sammis, C. G., & King, G. C. (2007). Mechanical origin of power law scaling in fault zone rock. *Geophysical Research Letters*, *34*(4).

Segall, P., & Rice, J. R. (1995). Dilatancy, compaction, and slip instability of a fluid-infiltrated fault. *Journal of Geophysical Research: Solid Earth*, *100*(B11), 22155–22171.

Segall, P., Rubin, A. M., Bradley, A. M., & Rice, J. R. (2010). Dilatant strengthening as a mechanism for slow slip events. *Journal of Geophysical Research: Solid Earth*, *115*(B12).

Shäfer, J., Dippel, S., & Wolf, D. (1996). Force schemes in simulations of granular materials. *Journal de physique I*, *6*(1), 5–20.

Silbert, L. E. (2010). Jamming of frictional spheres and random loose packing. *Soft Matter*, *6*(13), 2918–2924.

Silbert, L. E., Ertaş, D., Grest, G. S., Halsey, T. C., Levine, D., & Plimpton, S. J. (2001). Granular flow down an inclined plane: Bagnold scaling and rheology. *Physical Review E*, *64*(5), 051302.

Sleep, N. H. (1997). Application of a unified rate and state friction theory to the mechanics of fault zones with strain localization. *Journal of Geophysical Research: Solid Earth*, *102*(B2), 2875–2895.

Sleep, N. H. (2006). Real contacts and evolution laws for rate and state friction. *Geochemistry, Geophysics, Geosystems*, *7*(8).

Sleep, N. H., Richardson, E., & Marone, C. (2000). Physics of friction and strain rate localization in synthetic fault gouge. *Journal of Geophysical Research: Solid Earth*, *105*(B11), 25875–25890.

Song, C., Wang, P., & Makse, H. A. (2005). Experimental measurement of an effective temperature for jammed granular materials. *Proceedings of the National Academy of Sciences*, *102*(7), 2299–2304.

Tsai, J.-C., & Gollub, J. P. (2005). Granular packings sheared in an annular channel: Flow localization and grain size dependence. *Physical Review E*, *72*(5), 051304.

Tullis, T. E., & Weeks, J. D. (1986). Constitutive behavior and stability of frictional sliding of granite. *Pure and Applied Geophysics*, *124*(3), 383–414.

van der Elst, N. J., Brodsky, E. E., Le Bas, P.-Y., & Johnson, P. A. (2012). Auto-acoustic compaction in steady shear flows: Experimental evidence for suppression of shear dilatancy by internal acoustic vibration. *Journal of Geophysical Research: Solid Earth*, *117*(B9).

van Hecke, M. (2015). Slow granular flows: The dominant role of tiny fluctuations. *Comptes Rendus Physique*, *16*(1), 37–44.

Wortel, G., Dauchot, O., & van Hecke, M. (2016). Criticality in vibrated frictional flows at finite strain rate. *arXiv preprint arXiv:1603.04828*.

Wortel, G. H., Dijksman, J. A., & van Hecke, M. (2014). Rheology of weakly vibrated granular media. *Physical Review E*, *89*(1), 012202.

Yin, H. (1993). *Acoustic velocity and attenuation of rocks: Isotropy, intrinsic anisotropy, and stress-induced anisotropy* (Doctoral Dissertation). Stanford University.

Zhang, H., & Makse, H. (2005). Jamming transition in emulsions and granular materials. *Physical Review E*, *72*(1), 011301.

Supporting Information for "A granular-physics-based view of fault friction experiments"

Behrooz Ferdowsi[1], Allan M. Rubin[1]

[1]Department of Geosciences, Princeton University, Princeton, NJ 08544, USA

Contents of this file

1. More on the variation of steady-state friction with inertial number
2. The influence of the restitution coefficient
3. The influence of grain size
4. The influence of grain-grain friction coefficient
5. Figure S1
6. Figure S2
7. Figure S3
8. Figure S4
9. Figure S5
10. Figure S6

Corresponding author: B. Ferdowsi, Department of Geosciences, Princeton University, Princeton, NJ 08544, USA (behrooz@princeton.edu)

11. Figure S7

Introduction

This supplementary information file includes extended discussion of the results and supplementary figures for the variation of friction with inertial number, and the influences of restitution coefficient, grain size, and grain-grain friction coefficient, on the transient and steady-steady state frictional behavior of the sheared granular fault gouge. In this file, we also include a supplementary figure for the behavior of servo-controlled system during a velocity-step (Fig. S2), and another supplementary figure for the behavior of fault gouge with quasi-exponential grain size distribution in velocity-stepping tests (Fig. S7).

More on the variation of steady-state friction with inertial number

We would like to acknowledge that most other numerical studies use a power-law (local granular rheology of the form $\mu_{ss} - \mu_0 = c\, {I_n}^{\alpha}$) to describe the variation of friction with inertial number (or sliding speed) in their studies. However, relative to previous numerical studies, we explore a somewhat lower range of I_n (roughly $10^{-7} - 10^{-2}$, compared to $10^{-5} - 10^{0}$, which extends to well outside the quasi-static regime). While those previous studies found steady-state friction to have a power-law dependence upon I_n, they are nonetheless consistent with ours in that for the overlapping range of I_n ($\sim 10^{-5} - 10^{-2}$) they can be fit quite well by a logarithmic dependence of friction upon I_n, with a slope not much different than ours [e.g., Hatano, 2007]. It is for values of $I_n \gtrsim 10^{-2}$ in those studies, extending well into the inertial regime of flow, that the steady-state friction curve becomes obviously concave-upward. The steady-state results in Figure 2 of the main paper differ from previous simulations mostly in extending the range of I_n lower by ∼2 orders of magnitude. We find the logarithmic dependence to continue to those lower values, while the power-law fits (but not the data, since these don't extent to such low I_n) adopted by previous studies continue to flatten with decreasing I_n.

In Figure S1 below, we show a best fit logarithmic function to our friction data ($\mu_{ss} = c \log I_n + b$, where $c = 0.0055$ and $b = 0.403$) for the range of inertial numbers included for the default model in the paper Fig. 2 ($I_n < 5 \times 10^{-3}$). Although there is indeed some scatter in our data around this line for $I_n < 5 \times 10^{-3}$, it is not obvious that the data are more concave up (indicative of a power law) than concave down. Given this, we believe that an experimentalist would fit such data (for $I_n < 5 \times 10^{-3}$) with a logarithm rather than a power law, which has an additional free parameter. In this figure we also include the friction data of our default model for $I_n \geq 5 \times 10^{-3}$. These data are shown with filled black circles in Figure S1A. It is evident from this figure that at an inertial number $I \sim 10^{-2}$, the friction data start to deviate from the logarithmic fit and develop a concave-up shape. Figure S1B shows the friction data only for $I_n \geq 10^{-4}$. This is the range that is used for fitting a power-law function in the study by Hatano (2007) and Bouzid et al (2013). The black line in Fig. S1B shows a power-law fit ($\mu_{ss} - \mu_0 = c\, {I_n}^{\alpha}$, with $\mu_0 = 0.3538$, $c = 0.3981$ and $\alpha = 0.6562$) to these data. The parameters of this power-law fit fall between the range of parameters obtained by Hatano (2007) [$\mu_0 \approx 0.26$, $c = 0.33$, $\alpha = 0.3$ for his frictional Hertzian model with grain-grain friction coefficient of 0.2] and Bouzid et al. (2013) [$\mu_0 = 0.267$, $c = 1.148$, $\alpha = 1$ for the frictional Hookean model with grain-grain friction coefficient of 0.4]. Our default model is not identical to either of these studies, but the difference between these two published studies suggest that the power-law fit parameters can be expected to vary somewhat.

The influence of the restitution coefficient

Figs. S3A-B show the evolution of friction coefficient and gouge thickness, respectively, in a systems with the minimum value of restitution coefficient in this study ($e_n = 0.003$), and compare them to the behavior of the default model (with $e_n = 0.98$). The comparison is performed for $1 - 2$ orders of magnitude velocity-step increases and 1 order of magnitude velocity-step decrease. The results indicate that velocity-step response of the granular fault gouge is largely independent of the choice of the grain-grain restitution coefficient. A similar observation has been made for other values of the restitution coefficient that are explored here.

For the systems that are generated and confined with different restitution coefficients, we also measured the variations of kinetic energy and the ratio of kinetic energy to the total work done by shearing when shearing phase is initiated. The variations of friction coefficient, gouge thickness, and kinetic energy, as a function of slip distance, are shown in Figure S4A-C, respectively. Figure S4A shows that the choice of the restitution coefficient does not result in any macroscopically significant or any systematically observable change in bulk frictional behavior. The variation of gouge thickness with slip distance shows that in approach to steady-state, there might be subtle differences in gouge thickness in systems at the two ends of the damping regime. The system with minimum restitution coefficient (maximum damping) $e_n = 0.003$ appears to reach steady-state frictional behavior at a slightly more dilated state, compared to the system with maximum restitution coefficient (minimum damping) $e_n = 0.98$. However, these differences will disappear upon shearing for a longer distance, which is the point at which velocity-steps are performed.

The Kinetic Energy (KE) of the gouge layer is calculated from the sum of the kinetic translational and rotational energies, calculated and summed over all grains in the gouge layer:

$$KE = \sum_{i=1}^{n_p} \frac{1}{2} m_p v_p^2 + \sum_{i=1}^{n_p} \frac{1}{2} I_p {\omega_p}^2 \tag{1}$$

In Eq. 1, n_p is the total number of grains in the system, and m_p, I_p, v_p, and ω_p are the particle's mass, moment of inertia, translational, and angular velocities, respectively. Following the approach to steady-state friction, the variation of kinetic energy appears to be influenced to some small degree by the choice of the restitution coefficient. The systems with higher restitution coefficient ($e_n = 0.98$) and $e_n = 0.92$) appear to have a larger value of kinetic energy, while the systems with lower restitution coefficient show on average smaller values of kinetic energy.

The influence of grain size

We also ran velocity-step increase and decrease tests with a system with a grain and domain size two orders of magnitude smaller than the default model. The variation of friction and gouge thickness for these simulations are shown and compared to the behavior of the default model in Figure S5 A and B, respectively. The overall frictional and diltational behaviors of the two systems are similar. The critical slip distance in both cases is $D_c \sim 1.7 D_{mean}$. The system with two orders of magnitude smaller grain and domain sizes shows a slightly larger evolution effect compared to the default model in velocity-step increase tests. However, these variations could be potentially due to that the granular RSF parameters are influenced by the gravity forces that are active in this model. The gravity can change the anisotropic pressure state of the gouge more noticeably (although it is still a small contribution) in this "scaled-down" model compared to the default model.

The response of the gouge thickness in velocity step increase and decrease is shown in Figure S5B. These results also show that except for subtle differences in dilatational response, the behaviors are generally similar to the default model. Furthermore, as for the default model, the magnitude of gouge thickness change following velocity-step increase and decrease appears to be asymmetric, while the frictional response is nearly symmetric for both the default and the scaled-down model.

The influence of grain-grain friction coefficient

To examine the influence of grain-grain friction coefficient on the granular RSF behavior, we further performed velocity-step experiments with systems that are prepared with grain-grain friction coefficients of $\mu_g = 1.0$ and $\mu_g = 5.0$. We remind the reader that the grain-grain friction coefficient in our default model was $\mu_g = 0.5$. Figure S6A and B show the variation of friction coefficient and gouge thickness with slip distance, respectively, following $1-2$ and -1 orders of magnitude change in shear velocity in the system with $\mu_g = 1.0$. The results are compared to the behavior of the default model. Figure S6A-B show that frictional and dilatational responses of the system with $\mu_g = 1.0$ follow closely the behaviors of the default model. However, here we observe a larger amount of noise and fluctuations in the variation of friction coefficient with slip distance compared to the default model. The frictional and dilatational behaviors of the system with $\mu_g = 5.0$ are not shown here, but the behaviors remain similar to the default system, with even higher amounts of noise and larger fluctuations in friction coefficient signal.

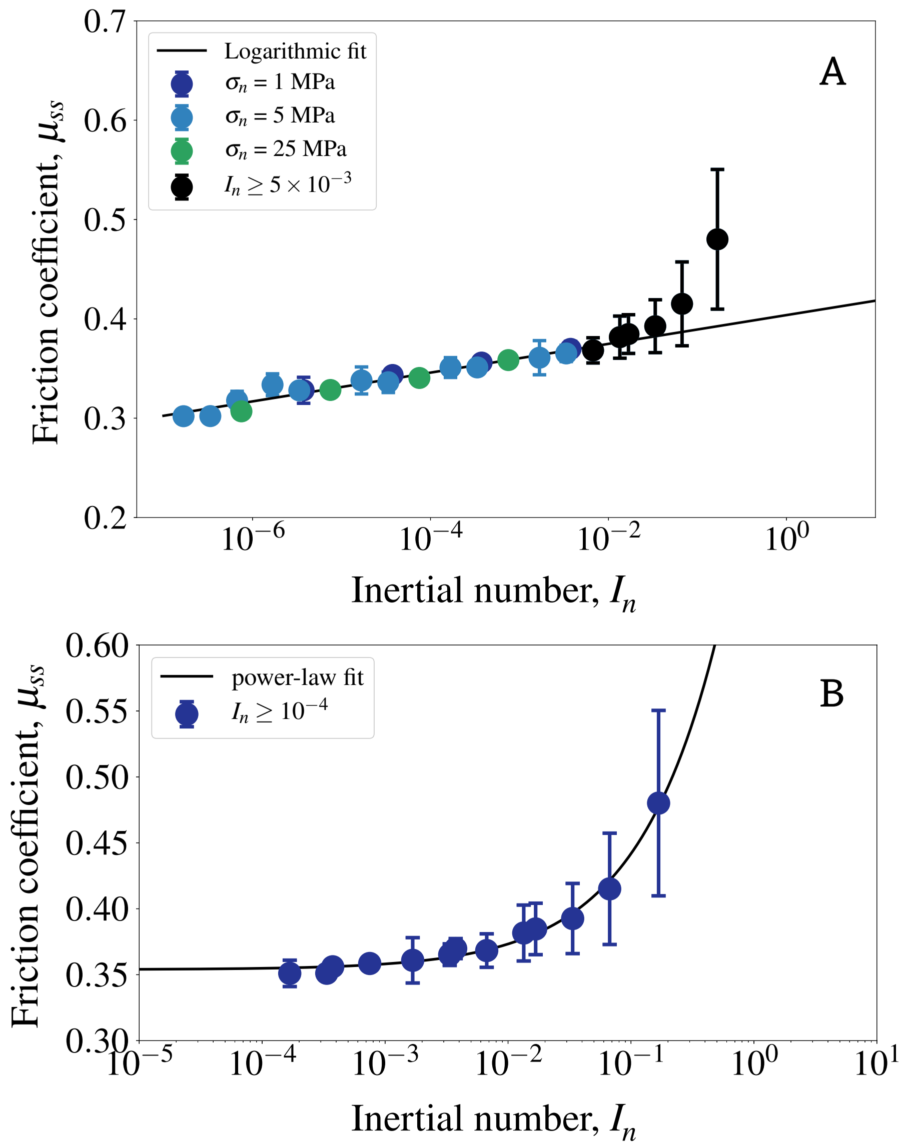

Figure S1. (A) The navy blue, light blue, and green filled circles show the variation of steady-state friction coefficient with inertial number (I_n) for the default system for the range of inertial numbers presented in the manuscript. The black circles show the steady-state friction coefficient with inertial number $I_n \geq 5 \times 10^{-3}$; these are beyond the range of inertial numbers shown in Fig. 2 of the manuscript. The black line shows a logarithmic best fit to the data shown in the paper ($I_n < 5 \times 10^{-3}$). (B) The variation of steady-state friction coefficient with I_n for the default system for $I_n \geq 1 \times 10^{-4}$. This is the range of inertial numbers used in the study by Hatano (2007) and several other granular physics studies for fitting a power-law to the data. The black line shows a power-law best-fit to the data, $\mu_{ss} - \mu_0 = c\, I_n{}^{\alpha}$. The values of the power-law parameters lie between the values found by Hatano (2007) and Bouzid et al. (2013).

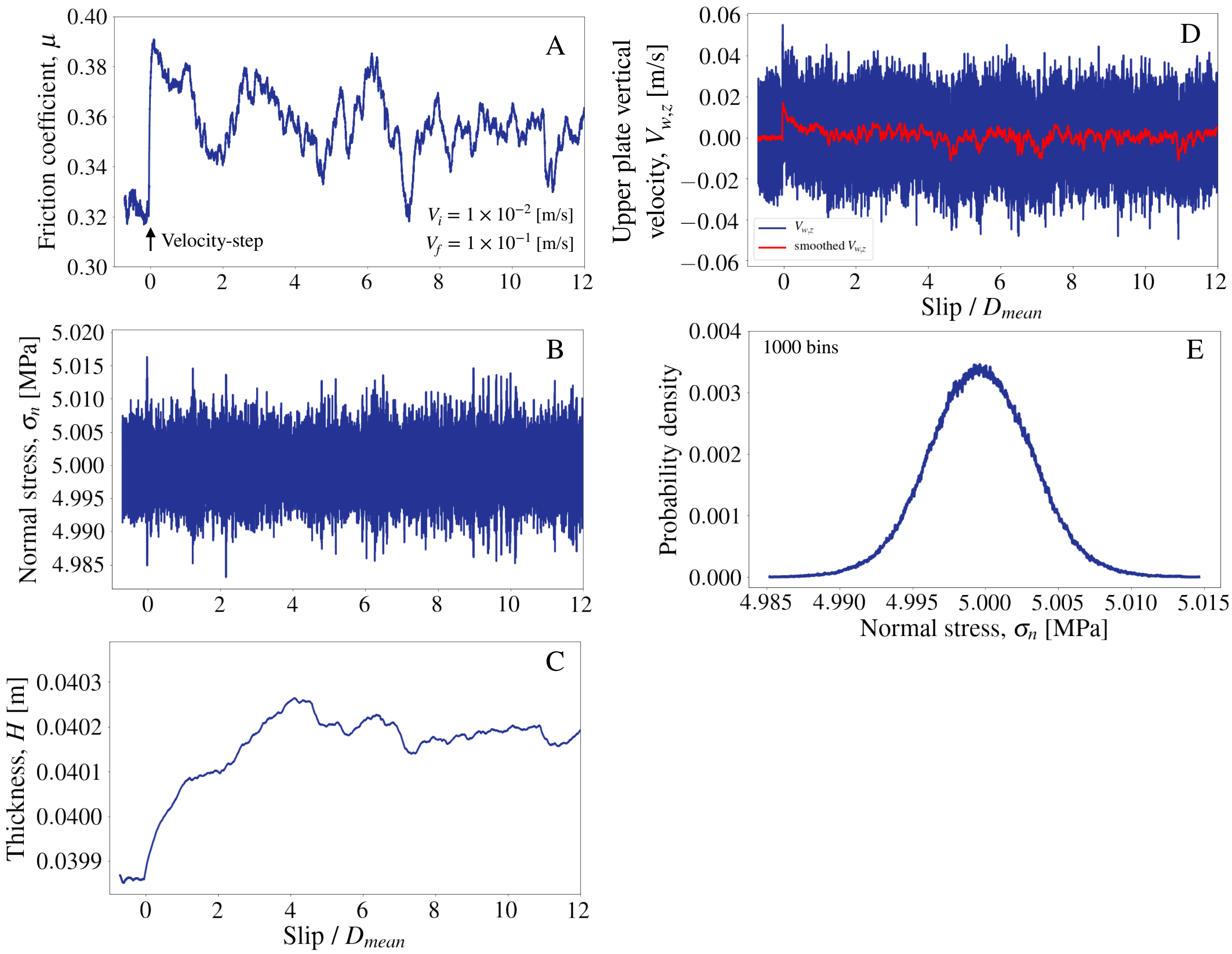

Figure S2. The variation of (A) friction, (B) normal stress, (C) gouge thickness, and (D) upper plate velocity, $V_{w,z}$, with slip distance, in a velocity-stepping test with the initial sliding velocity of $V_i = 10^{-2}$ m/s and the final sliding velocity of $V_f = 10^{-1}$ m/s. Panel (E) shows the probability distribution of normal stress during steady-sliding at $V_f = 10^{-1}$ m/s, for sliding distance $5 \leq \text{Slip}/D_{mean} \leq 12$. All of the signals are sampled every 10 time-steps in the simulation. The smoothed upper plate velocity, $V_{w,z}$ (red line in panel D) is obtained with a moving average with window size $0.01 D_{mean}$.

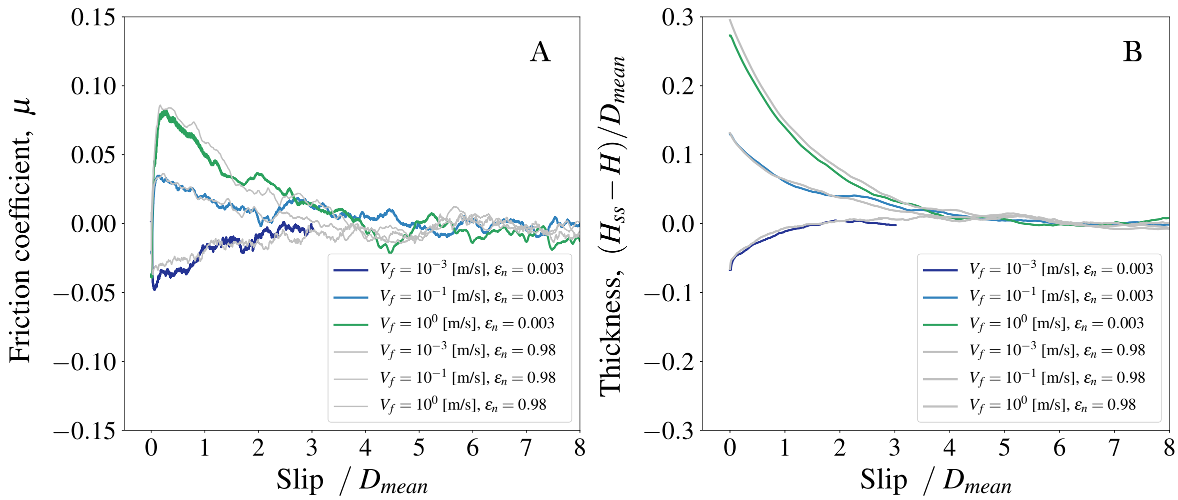

Figure S3. The influence of restitution coefficient on velocity-steps. Panels (A) and (B) show the variation of friction coefficient and gouge thickness with slip distance, respectively, in simulations with $1-2$ and -1 orders of magnitude change in shear velocity. The initial driving velocity in all tests is $V_i = 10^{-2}$ m/s. The colored lines are simulation results for the system with the restitution coefficient $e_n = 0.003$, whereas the gray lines are the results for the system with $e_n = 0.98$. The results are averaged over seven different realizations. The normal stress is fixed at 5 MPa in all tests.

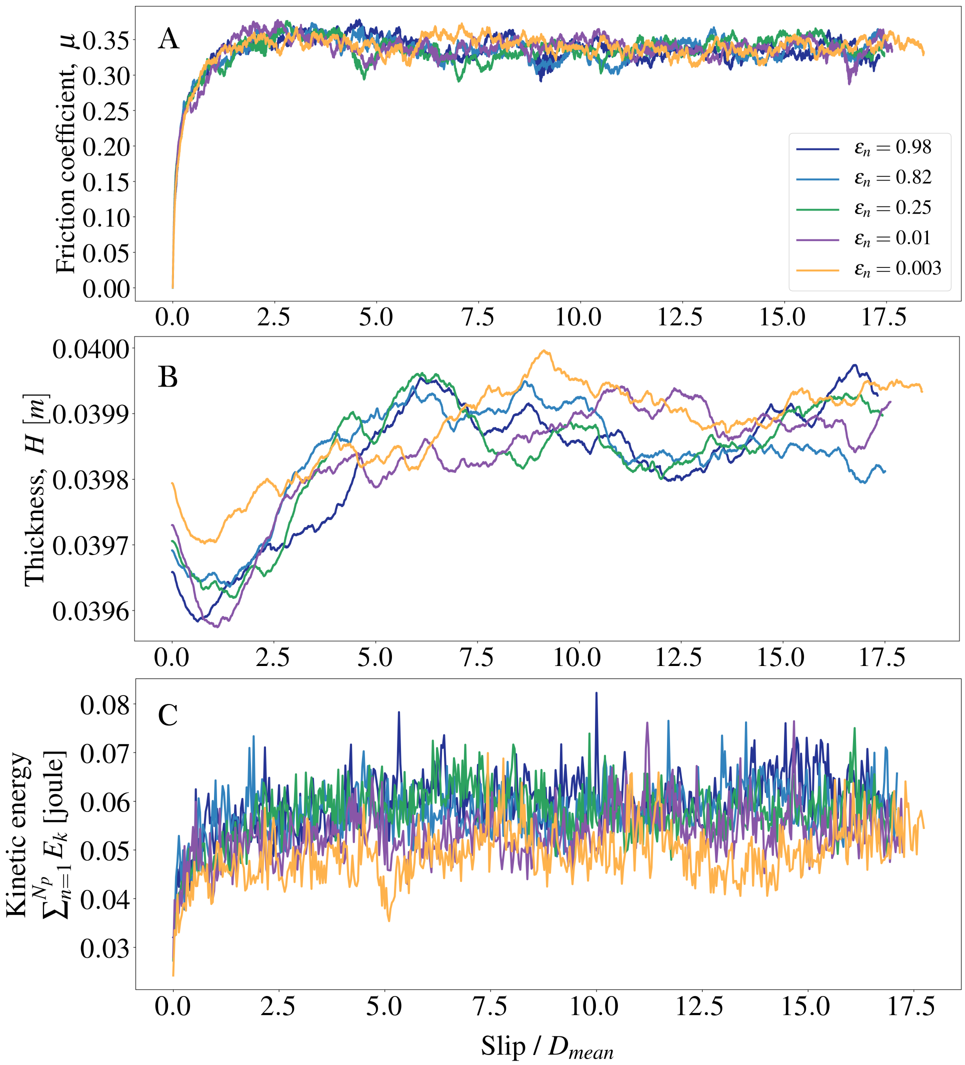

Figure S4. The variation of (A) friction coefficient, (B) gouge thickness, (C) kinetic energy with slip distance for different values of restitution coefficient. The results are only for one realization of the system. The driving velocity is $V_{lp} = 1 \times 10^{-2}$ m/s and the normal stress is fixed at 5 MPa in all simulations.

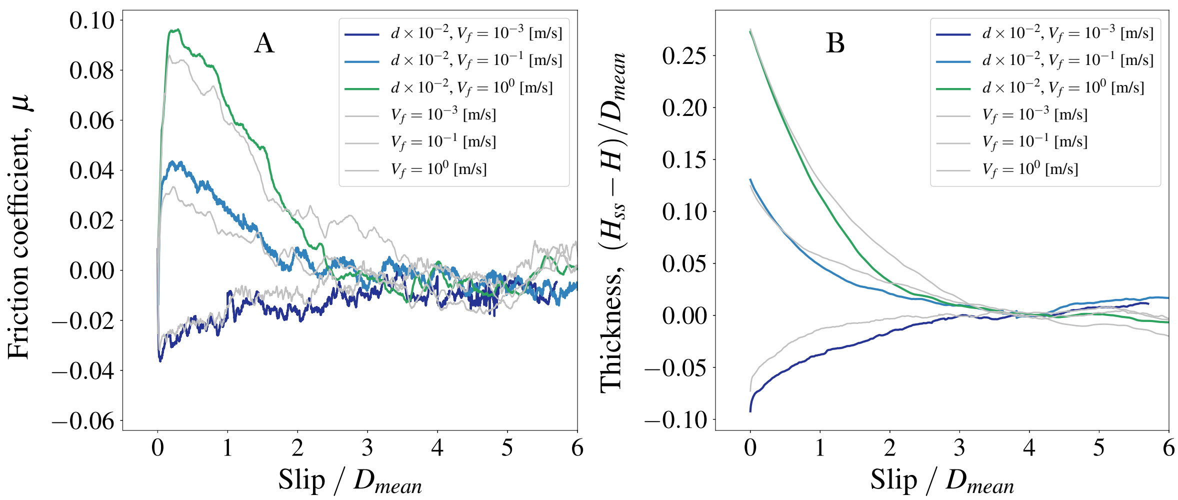

Figure S5. The influence of grain size. Panels (A) and (B) show the variation of friction coefficient and gouge thickness with slip distance, respectively, in simulations with $1-2$ and -1 orders of magnitude change in shear velocity. The initial driving velocity in all tests is $V_i = 10^{-2}$ m/s. The colored lines are simulation results for the system where grain size is scaled down by two orders of magnitude. The gray lines show the results for the default model. All results are averaged over seven different realizations. The normal stress is fixed at 5 MPa in all tests.

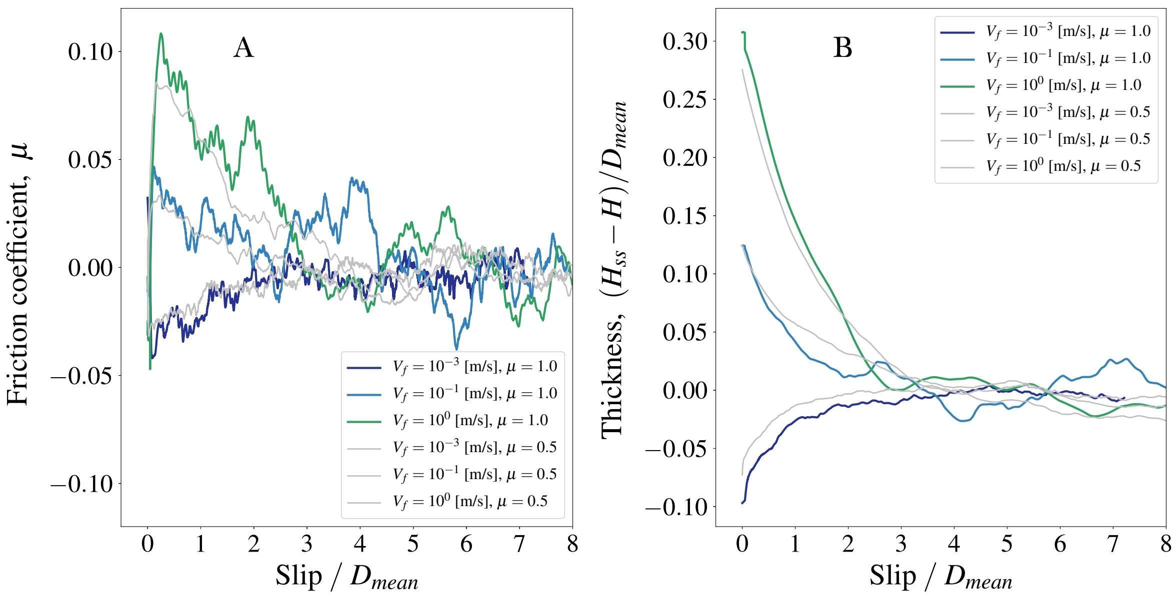

Figure S6. The influence of grain-grain friction coefficient. Panels (A) and (B) show the variation of friction coefficient and gouge thickness with slip distance, respectively, in simulations with $1-2$ and -1 orders of magnitude change in shear velocity. The initial driving velocity in all tests is $V_i = 10^{-2}$ m/s. The colored lines are simulation results for the system where grain-grain friction coefficient is $\mu_g = 1.0$. The gray lines show the results for the default model. All results are averaged over seven different realizations. The normal stress is fixed at 5 MPa in all tests.

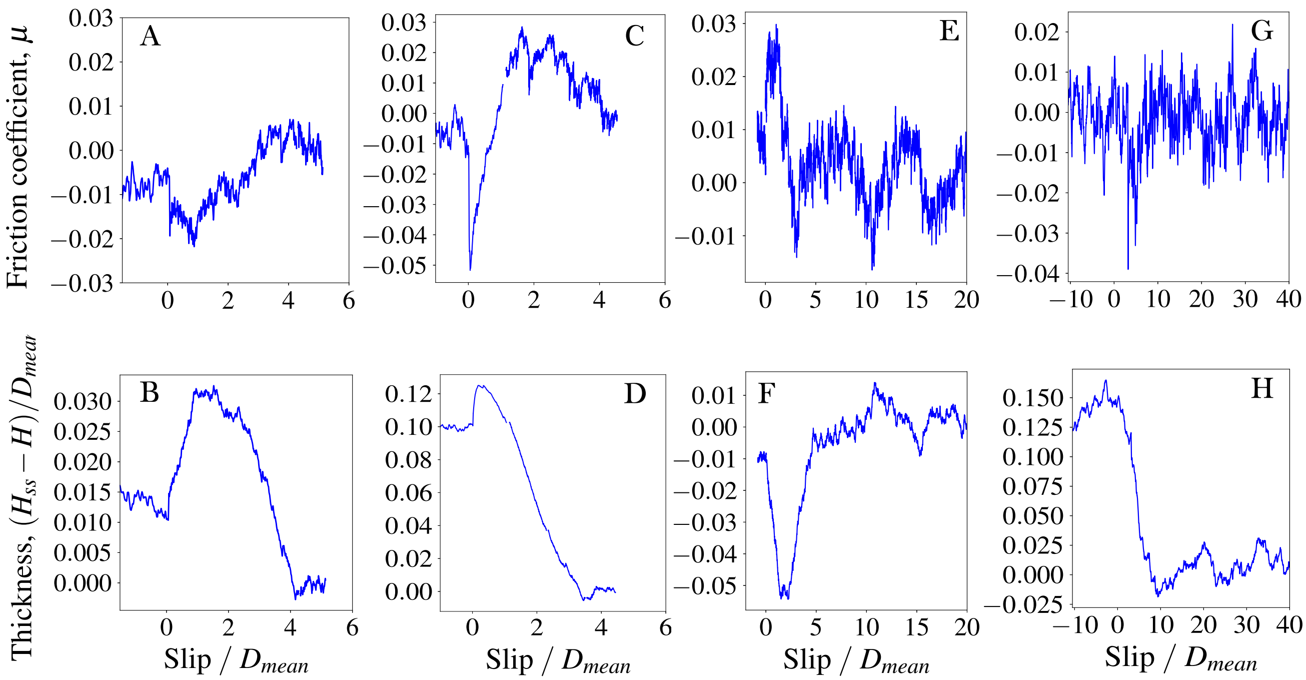

Figure S7. Results of simulations with a quasi-exponential grain size distribution. The top panels (A-C-E-G) show the variation of friction coefficient and the bottom panels (B-D-F-H) show the variation of gouge thickness with slip distance. Panels A-B show results for a 1-order velocity step decrease from $V_i = 10^{-1}$ m/s. Panels C-D show a 2-order step decrease from the same initial velocity. Panels E-F show results for a 1-order velocity step increase from $V_i = 10^{-2}$ m/s. Panels G-H show results for a 1-order step decrease from $V_i = 1$ m/s. $\sigma_n = 5$ MPa. All panels, except G-H, average results from three different realizations; G-H are from a single realization.